Reactions of $Cp_2Ta(CH_2)(CH_3)$ with Substituted and Unsubstituted Metal Carbonyls (Groups 7, 8, and 9). Evidence for Intermediates Involved in the Carbon−Carbon Bond-Forming Steps of the Reduction and Deoxygenation of CO

Grant Proulx‡ and Robert G. Bergman*

Contribution from the Department of Chemistry, University of California, Berkeley, California 94720-1460

Received May 24, 1995. Revised Manuscript Received November 29, 1995[⊗]

Abstract: The mechanisms of surface-catalyzed reactions that deoxygenate carbon monoxide (CO) and convert it into longer chain hydrocarbons are not well understood. Homogeneous models involving soluble, well-characterized organometallic complexes would be helpful in developing an understanding of these reactions. Reported here are transformations in which CH_2, CO, alkyl, and aryl fragments incorporated in soluble metal complexes undergo a variety of changes that lead to new multicarbon ligands. In one example, treatment of the tantalum methylene complex $Cp_2Ta(CH_2)(CH_3)$ (**1**, Cp = η^5-C_5H_5) with the methyl- or phenylrhenium pentacarbonyl complexes R−Re-$(CO)_5$ (R = CH_3 (**2a**), Ph (**2b**)) above 0 °C leads to >90% yields of the bridging oxo complexes $Cp_2(CH_3)Ta(\mu$-O)Re$(CR{=}CH_2)(CO)_4$ (R = Me (**3a**) and Ph (**3b**)). Low-temperature NMR monitoring and use of a perfluoroalkyl ligand has provided information about the initial steps in these transformations. These demonstrate the first observation of "Wittig-like" attack of a metal alkylidene group on a CO ligand to give a zwitterion (e.g., fully characterized **16**) followed by cleavage to oxometal and vinylidene complexes. In another example, the tantalum−methylene complex **1** reacts with the dinuclear metal carbonyls $Co_2(CO)_8$ and $Fe_2(CO)_9$ to yield new complexes (**17** and **18**) that incorporate a $C_3H_2O_2$ ligand bridging three metal centers. Reaction of the tantalum−methylene complex with $Re_2(CO)_{10}$, Mn_2-$(CO)_{10}$, or $Fe(CO)_5$ leads to **19**, **20**, and **21**, requiring even more deep-seated changes in which extensive rearrangement along with three-carbon coupling occurs. In this process, an oxygen atom is removed from one CO group, leading to the oxotantalum compound $Cp_2(CH_3)Ta{=}O$. The carbon atom from the transformed CO couples with two CH_2 groups initially bound to tantalum, and the CH_2 hydrogens are simultaneously rearranged to produce a $CH_3{-}C{\equiv}C^-$ ligand. This C_3 fragment is stabilized by binding to a tantalum−late-metal chain. These products also contain the first examples of tantalum−carbon monoxide bridges. A reaction between **1** and $Ru_3(CO)_{12}$ that results in CO deoxygenation along with coupling of the CO carbon to methylidene groups and other CO carbons to yield the cluster complex $Cp_2(CH_3)Ta(\mu$-O)$Ru_3(C_4H_4)(CO)_9$ (**23**) and the unstable free tantalum oxo species $Cp_2Ta(=O)$-(CH_3) is also reported. The $TaRu_3$ product contains a 4-carbon cumulene ligand that bridges the three late-metal centers. The crystal structures of complexes **3b**, **16**, **17**, **18**, **19**, **20**, **21**, and **23** are reported.

The reduction of carbon monoxide and its incorporation into longer-chain hydrocarbons is one of the most intensely studied fields in organotransition metal chemistry. An example of such a transformation, the heterogeneous Fischer−Tropsch process,[1] converts synthesis gas (CO/H_2) into an array of products including a number of differing hydrocarbons, olefins, alcohols, aldehydes, acids, and aromatics. Its mechanism is still not well understood, but a proposed initial step involves attack of a nucleophilic transition metal hydride on an electrophilic metal carbonyl.[2] This leads to a formyl complex that is believed to decompose to a metal oxide (which is later given off as H_2O) and a surface-bound methylidene fragment. Oligomerization of methylidene fragments is thought to be responsible for many of the chain growth products observed in the F-T process.

Carbon monoxide reduction and oligomerization processes that occur in homogeneous solution are more amenable to detailed mechanistic study and presumably would provide information relevant to analogous heterogeneous processes. A number of soluble complexes have been found that convert CO and H_2 into methanol, and a few homogeneous solution reactions are known in which CO molecules are coupled[3−6] or cleaved.[7−9] However, homogeneous CO oligomerization processes are still rare. Organometallic reactivity relevant to the dissociative cleavage of CO is observed in certain metal carbonyl clusters and low-valent early transition metal species, but external reagents are often needed to form C−C bonds from the resulting carbides. Conversely, early transition metal and actinide hydride complexes model CO reduction and C−C bond-forming reactions, yet few examples of C−O bond scission have been observed. Other systems have used highly electronically unsaturated early-metal species to cleave the C≡O bond of free carbon monoxide.

‡ Present address: DuPont Nylon, Experimental Station, P.O. Box 80302, Rm E302-2210, Wilmington DE 19880-0302.

⊗ Abstract published in *Advance ACS Abstracts,* January 15, 1996.

(1) Muetterties, E. L.; Stein, J. *Chem. Rev.* **1979**, *79*, 479.
(2) Wong, K. S.; Labinger, J. A. *J. Am. Chem. Soc.* **1980**, *102*, 3652.
(3) Anslyn, R. V.; Santarsiero, B. D.; Grubbs, R. H. *Organometallics* **1988**, *7*, 2137.
(4) Wood, C. D.; Schrock, R. R. *J. Am. Chem. Soc.* **1979**, *101*, 5421.
(5) Carnahan, E. M.; Lippard, S. J. *J. Am. Chem. Soc.* **1992**, *114*, 4166 and references cited there.
(6) Bercaw, J. E.; Sanner, R. D.; McAlister, D. R.; Manriquez, J. M. *J. Am. Chem. Soc.* **1978**, *100*, 2716.
(7) Toreki, R.; LaPointe, R. E.; Wolczanski, P. T. *J. Am. Chem. Soc.* **1987**, *109*, 7558.
(8) Neithamer, D. R.; LaPointe, R. E.; Wheeler, R. A.; Richeson, D. S.; Van Duyne, G. D.; Wolczanski, P. T. *J. Am. Chem. Soc.* **1989**, *111*, 9056.
(9) Miller, R. L.; Toreki, R.; LaPointe, R. E.; Wolczanski, P. T.; Van Duyne, G. D.; Roe, C. C. *J. Am. Chem. Soc.* **1993**, *115*, 5570.

0002-7863/96/1518-1981$12.00/0

We have recently published preliminary information on a series of reactions between $Cp_2Ta(CH_3)(CH_2)$ (the first stable transition metal methylene complex[10]) and a number of metal carbonyls and their derivatives.[11,12] In this full report, we describe Ta-mediated processes that couple CO and CH_2 as well as alkyl, alkenyl, and aryl groups in homogeneous solution. These reactions occur at or below ambient temperatures and in the absence of light, and lead to an array of products whose identities depend on the metal center and the ligand environment. This appears to be the first detailed study of homogeneous reactions that utilize the vastly different electronic properties available from the early and late-metal series in which extensive CO bond reduction and cleavage is observed along with incorporation of the carbonyl carbon into an array of CH- and CHO-containing products. We have accomplished the spectroscopic identification and isolation of several intermediates, which has led to progress in our understanding of how these transformations occur.

Results

Reaction of $(\eta^5\text{-}C_5H_5)_2Ta(CH_2)(CH_3)$ with the Hydrocarbon-Substituted Metal Carbonyls $(CH_3)Re(CO)_5$ and $(C_6H_5)Re(CO)_5$. The reaction between the tantalum methylidene complex, $Cp_2Ta(CH_2)(CH_3)$[10] ($Cp = \eta^5\text{-}C_5H_5$) (**1**), and the hydrocarbyl-substituted rhenium pentacarbonyl complexes occurs rapidly and in good yield in a variety of solvents even at significantly reduced temperatures.

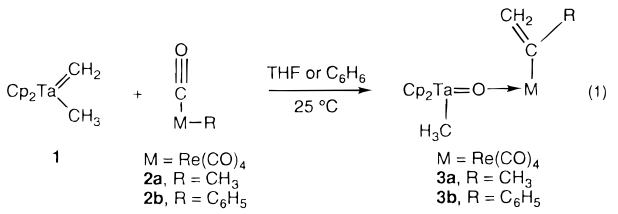

For example, treatment of a THF solution of **1** with 1 equiv of the methyl- or phenylrhenium pentacarbonyl complexes R−Re(CO)$_5$ (R = CH_3 (**2a**), Ph (**2b**)) yielded gold to yellow compounds with the general formula $Cp_2(CH_3)Ta(\mu\text{-}O)Re(CR{=}CH_2)(CO)_4$ (R = Me (**3a**) and Ph (**3b**))[13,14] (eq 1). This reaction occurs at room temperature and in the absence of light, requiring only seconds to provide a high yield of product (>90% by ^{1}H NMR spectroscopy). Compounds **3a** and **3b** were isolated in 61% and 67% yield, respectively, in pure crystalline form by slow diffusion of pentane into a benzene solution followed by slow cooling to −30 °C. The ^{1}H NMR spectrum of the product, **3b**, suggested its identity as an alkenyl complex by showing two doublets attributable to inequivalent vinylic protons, and the $^{13}C\{^1H\}$ NMR spectrum also showed resonances consistent with a new phenyl-substituted vinyl group bound to Re. The IR spectra of **3a** and **3b** have absorbances at 833 and 831 cm^{-1}, respectively, which we assign to Ta−O−Re bridging oxo stretches.

To confirm these inferences, an X-ray crystallographic analysis of **3b** was performed (see Table 1, Figure 1). This revealed a heterobimetallic structure in which there was a bridging oxo group along with a new α-styryl group bound to the late metal. The Re center has a pseudo-octahedral coordination geometry, with the styryl group cis to the bridging oxide unit. The CH_2 group of the styryl ligand is directed toward the Cp_2Ta center and the more sterically demanding phenyl group directed away from it. The bonding situation regarding the bridging oxo ligand is a little more unusual. The length of the Ta=O bond was found to be 1.761(11) Å, while the Re−O bond is 2.147(11) Å,[15] suggesting that the complex possesses a Ta=O double bond and a Re−O donor−acceptor interaction. The Ta−O−Re bond angle of 179.0(6)° is nearly linear. A linear structure with a large difference in metal−oxo bond lengths between an early and a late transition metal is rare but is generally viewed[16] as being due to a dative interaction between oxygen and the metal center. Formally, this makes an 18e$^-$ Ta(V) and an 18e$^-$ Re(I) species which is consistent with the diamagnetic character of **3b**. Also, there does not appear to be any bonding interaction between the vinyl fragment

Table 1. Selected Intramolecular Distances and Angles for $Cp_2Ta(CH_3)(\mu\text{-}O)Re(C(CH_2)Ph)(CO)_4$ (**3b**)

	Distance (Å)		
Re−O5	2.147(11)	C1−O1	1.191(19)
Re−C1	1.922(17)	C2−O2	1.159(19)
Re−C2	1.972(17)	C3−O3	1.176(19)
Re−C3	1.938(16)	C4−O4	1.195(18)
Re−C4	1.865(17)		
Re−C16	2.234(17)	C16−C17	1.34(2)
		C16−C18	1.47(2)
Ta−O5	1.761(11)	C18−C19	1.41(2)
		C18−C23	1.40(2)
Ta−C5	2.214(17)		
Ta−CP1	2.124		
Ta−CP2	2.149		
	Angle (deg)		
O5−Re−C16	87.0(5)	Re−O5−Ta	179.0(6)
C2−Re−C16	85.3(6)		
C3−Re−C16	87.5(6)	C17−C16−C18	116.6(15)
C4−Re−C16	93.9(7)	C16−C18−C19	120.9(14)
		C16−C18−C23	119.2(14)
O5−Ta−C5	94.4(6)	C19−C18−C23	119.9(14)
CP1−Ta−Cp2	128.3		

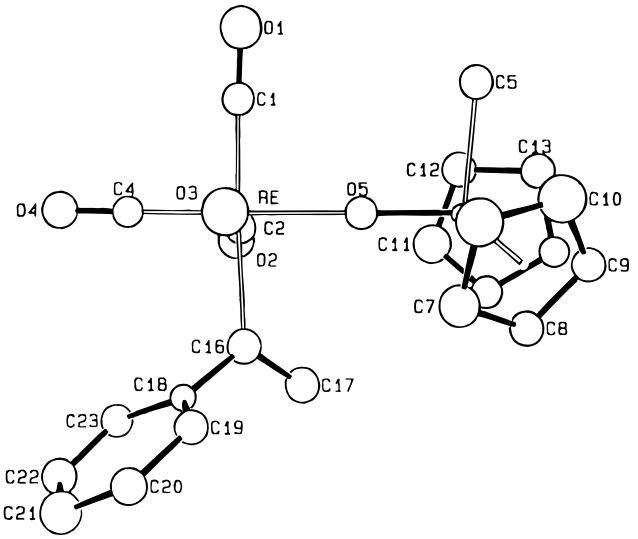

Figure 1. ORTEP diagram of $Cp_2(CH_3)Ta(\mu\text{-}O)Re(CPh{=}CH_2)(CO)_4$ (**3b**).

(10) Schrock, R. R.; Sharp, P. R. *J. Am. Chem. Soc.* **1978**, *100*, 2389.
(11) Proulx, G.; Bergman, R. G. *Science* **1993**, *259*, 661.
(12) Proulx, G.; Bergman, R. G. *J. Am. Chem. Soc.* **1993**, *115*, 9802.
(13) Fryzuk, M. D.; Huang, L.; McManus, N. T.; Paglia, P.; Rettig, S. J.; White, G. S. *Organometallics* **1992**, *11*, 2979.
(14) Selnau, H. E.; Merola, J. S. *J. Am. Chem. Soc.* **1991**, *113*, 4008.
(15) Herrmann, W. A.; Fischer, R. W. *J. Am. Chem. Soc.* **1995**, *117*, 3223.
(16) The formation of a bridging oxo complex by displacement of a solvent molecule from a late-metal species by the oxo ligand of an early-metal center has been documented before; see: Pilato, R. S.; Rubin, D.; Geoffroy, G. L.; Rheingold, A. L. *Inorg. Chem.* **1990**, *29*, 1986 and references cited there.

Scheme 1

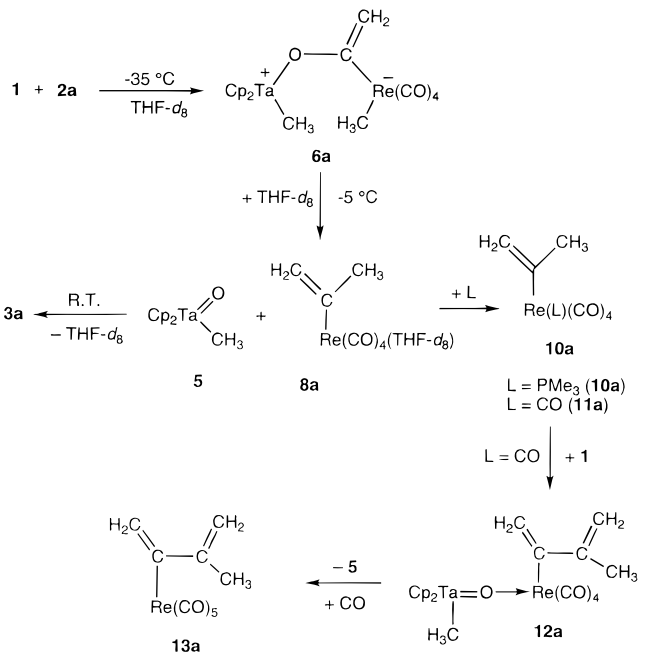

and the tantalum center which is consistent with the linearity about the oxygen atom.

Isotope tracer and low-temperature NMR monitoring experiments have also been performed. Reaction of $CD_3Re(CO)_5$ (**2a-*d*$_3$**) (eq 2) with **1** produced $Cp_2(CH_3)Ta(\mu\text{-}O)Re(CCD_3{=}CH_2)(CO)_4$ (**3a-*d*$_3$**) (>98% trideuterated), demonstrating that the vinyl methyl group is derived essentially exclusively from the $Re(CH_3)$ rather than the $Cp_2Ta(CH_2)(CH_3)$ center. A solution of

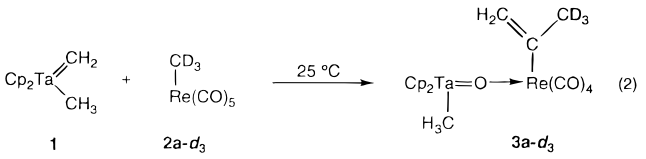

(2)

1 and **2a** were mixed in a sealed NMR tube at −50 °C and then warmed slowly. At −35 °C, the ^{1}H NMR spectrum showed the formation of a new material whose concentration builds up only at low temperature. The ^{1}H NMR spectrum was consistent with zwitterion[6] **6a**. The methyl proton resonance at −0.49 ppm shows that this group has not yet migrated away from the metal center (Scheme 1). At −5 °C this first observable intermediate began to decompose and two new thermally unstable products began to appear. One is the previously characterized oxotantalum complex $Cp_2(CH_3)Ta{=}O$ (**5**).[11,12] Details of the characterization of compound **5** are provided in another paper.[17] NMR data on the second of these products is consistent with its assignment as the 2-propenylrhenium THF-d_8 complex $(CO)_4Re(CMe{=}CH_2)(THF\text{-}d_8)$ (**8a**).[4] Upon further warming, resonances for **5**, **6a**, and **8a** disappear as resonances for the isolable product **3a** begin to appear.[12] At room temperature the only product remaining was **3a** in >90% yield.

We also monitored the reaction of **1** with **2a** in the presence of excess PMe_3 by ^{1}H NMR at several sub-ambient temperatures (Scheme 1). At −35 °C we observed that zwitterion **6a** formed again at a rate comparable to that observed in the absence of phosphine. Subsequently, at −5 °C, $CH_3C(CH_2)Re(CO)_4(PMe_3)$ (**10a**) (87% by ^{1}H NMR) and additional free $Cp_2(CH_3)Ta(=O)$ (**5**) are produced in place of THF complex **8a** and bridging oxo complex **3a**. Similarly, $CH_3C(CH_2)Re(CO)_5$ (**11a**) (91%) appears in place of **10a** if excess CO is used in place of phosphine. Also, upon treatment of $Cp_2(CH_3)Ta(=O)Re(CH_3C(CH_2))(CO)_4$ (**3a**) with carbon monoxide, the tantalum−oxo linkage can readily be displaced to form $CH_3C(CH_2)Re(CO)_5$ (**11a**) and $[Cp_2(CH_3)Ta{=}O]_n$ (which precipitates from a room temperature solution as a polymeric white flocculent powder and cannot be redissolved in common organic solvents). This demonstrates that the Ta(=O)→Re linkage is a relatively weak $2e^-$ donor−acceptor bond. We have synthesized $CH_3C(CH_2)Re(CO)_5$ (**11a**) and $CH_3C(CH_2)Re(CO)_4(PMe_3)$ (**10a**) independently (see Experimental Section) and the spectroscopic characterizations match those of the vinylrhenium carbonyl complexes generated above.

We have extended the vinyl chain by two more carbons via deoxygenation of another carbonyl in $CH_3C(=CH_2)Re(CO)_5$ (**11a**) (Scheme 1). Treating **11a** with more $Cp_2Ta(=CH_2)(CH_3)$ (**1**) leads to $Cp_2(CH_3)Ta(=O)Re(CH_3(C(CH_2))_2(CO)_4$ (**12a**) (73%). Upon further treatment of this new species with CO, the rhenium pentacarbonyl complex $CH_3(C(CH_2))_2Re(CO)_5$ (**13a**) can be regenerated with the appearance of a polymeric tantalum−oxo species. This rhenium-bound 3-methyl-2-butadienyl species appears to be quite stable thermally, but can undergo further attack by more tantalum methylidene **1**. We have repeated this sequence and spectroscopically characterized the chain-extended product through three of these transformations, but continued NMR observation indicates that the chain growth continues beyond this point (ca. 50−60%). We have not established the limit for this process. However, it appears that growth of the methyl-capped isomer of polyacetylene generated by the repeating sequence is assisted by the tendency for the tantalum oxide to precipitate from solution as a polymer so that it does not build up in large concentration at room temperature.

This deoxygenation/polymerization of carbon monoxide does appear to have certain limits with respect to ligand environment about the rhenium center. A second deoxygenation of carbon monoxide by **1** does not appear to occur unless and until the Ta=O linkage is replaced by a CO ligand. One can also successfully shut further reaction down by allowing a good electron donating group (such as phosphines) to coordinate to the rhenium center. It appears with this (and most other systems reported here) that phosphines (with the exception of PF_3) and other electron donating groups on the late-metal center will shut down the reaction between **1** and the metal carbonyls.

Isolation of a Zwitterionic Intermediate in the Reaction of (η^5-C_5H_5)$_2$Ta(CH$_2$)(CH$_3$) with (CF$_3$CF$_2$CF$_2$)Re(CO)$_5$. In an attempt to further understand the mechanism of the CH_2/O metathesis reaction that occurs between the tantalum methylidene complex and the substituted rhenium pentacarbonyl complexes, we attempted to use the known stability of perfluorinated alkylrhenium species to isolate and characterize an intermediate analogous to the one seen in low-temperature spectroscopic experiments between **1** and $RRe(CO)_5$.

The reaction between $Cp_2Ta(CH_2)(CH_3)$ (**1**) and $C_3F_7Re(CO)_5$ (**15**) proceeds in a fashion similar to those described for the alkyl- and aryl-substituted complexes (**3a** and **3b**) at low temperature (see eq 3). Upon mixing a THF-d_8 solution of **1**

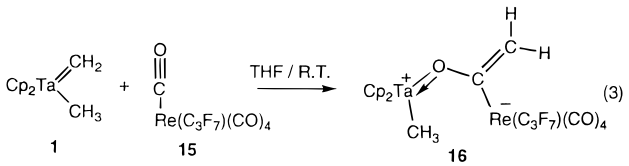

(3)

and **15** at −50 °C and slowly warming to −30 °C in a cooled

(17) Proulx, G.; Bergman, R. G. *Organometallics* **1996**, *15*, 133.

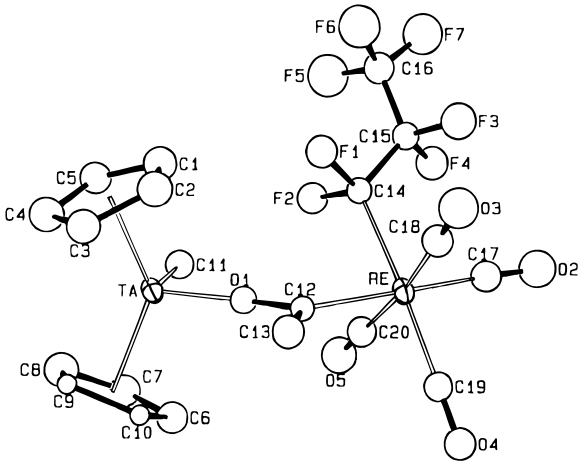

Figure 2. ORTEP diagram of $Cp_2(CH_3)Ta(\mu\text{-}OC_2H_2)Re(C_3F_7)(CO)_4$ (**16**).

Table 2. Selected Intramolecular Distances and Angles for $Cp_2(CH_3)Ta(OC(CH_2))Re(C_3F_7)(CO)_4$ (**16**)

	Distance (Å)		
Re−C12	2.192(12)	C12−O1	1.387(14)
Re−C14	2.206(12)	C12−C13	1.366(17)
Re−C17	1.932(15)		
Re−C18	1.991(13)	C17−O2	1.184(17)
Re−C19	1.966(13)	C18−O3	1.148(15)
Re−C20	1.949(13)	C19−O4	1.140(14)
		C20−O5	1.191(16)
Ta−O1	1.838(8)	C14−C15	1.538(17)
Ta−C11	2.212(13)	C14−F1	1.397(14)
		C14−F2	1.415(14)
TA−CP1	2.087		
TA−CP2	2.115		
	Angle (deg)		
C12−Re−C14	84.9(4)	Ta−O1−C12	160.8(8)
C12−Re−C17	179.6(5)	Re−C12−O1	117.8(8)
C12−Re−C18	85.5(5)	Re−C12−C13	127.7(9)
C12−Re−C19	91.1(5)	O1−C12−C13	114.4(11)
C12−Re−C20	87.9(5)		
C14−Re−C17	94.7(5)	Re−C14−F1	114.8(7)
C14−Re−C18	86.7(5)	Re−C14−F2	114.0(7)
C14−Re−C19	176.0(5)	Re−C14−C15	119.3(8)
C14−Re−C20	89.1(5)		
		F1−C14−F2	102.0(9)
Cp1−Ta−CP2	132.93(3)	F1−C14−C15	103.2(9)
O1−Ta−C11	97.3(4)	F2−C14−C15	101.2(9)
		C14−C15−C16	120.4(11)

probe while monitoring by ^{1}H NMR, a new product (**16**) is observed which has spectroscopic characteristics nearly identical to those observed in similar reactions with the alkyl-substituted species at that temperature. The inequivalent proton resonances for this complex now appear at δ 4.46 and 4.14 ppm which is in the proper range for an uncoordinated alkene (as compared to δ 4.32 and 3.82 ppm for the TaReMe (**6a**) intermediate). However, upon warming to 20 °C, formation of free $Cp_2Ta(=O)(CH_3)$ (**5**) or its polymer is not observed. By not allowing this solution to warm past 20 °C (<10 °C is ideal), it was possible to isolate and recrystallize this complex at subambient temperature to obtain pure, golden-yellow crystals of **16** in 73% yield.[18] The complex was characterized by X-ray diffraction (Figure 2; Table 2).

The bridging ketene ligand in this product formally arises by insertion of a bound carbon monoxide ligand into the $Ta{=}CH_2$ double bond. There is some disorder in one of the Cp rings bound to tantalum. The Re center is psuedo-octahedral with the C_3F_7 ligand oriented cis with respect to the C_2H_2O bridging ligand. The rhenium−carbon linkage to the ketene bridge appears to be a normal single bond ($Re-CCH_2$ is 2.192(12) Å). The C−O (1.387(14) Å) and $C{=}CH_2$ (1.366(17) Å) distances are in the normal range for a C−O single and C=C double bond, respectively. The Ta−O distance (1.838(8) Å) is significantly shorter than that in some related complexes with a "true" Ta−O single bond. The Ta−O single bond distances in the $Cp^*_2Ta(\eta^2\text{-}O_2)CH_2C_6H_5$ moiety are 1.996(6) and 1.955(6) Å,[19] and the Ta=O distance in **3b** (Ta(=O)−Re) is 1.761(11) Å. Thus, the formal bonding scheme appears to be consistent with a Ta−O single bond with considerable back-donation to the tantalum center by one or both lone pairs on the oxygen. A second lone pair interaction is possible considering that the Ta−O−C linkage is not far from linear at 160.8(8)° even though the tantalum would be formally 18e$^-$ with only a single interaction (this is quite a common occurrence and is well-documented in some related tantalum imido complexes).[20] The angle with respect to this linkage also makes any $Ta-CH_2$ interaction (which would formally lead to an oxametallacyclobutane) unlikely.

Reaction of $(\eta^5\text{-}C_5H_5)_2Ta(CH_2)(CH_3)$ with the Dinuclear Metal Carbonyls $Co_2(CO)_8$ and $Fe_2(CO)_9$. Complex **1** reacts with dinuclear metal carbonyls having relatively short metal−metal bond lengths (≤2.54 Å). These reactions occur rapidly even at low temperatures in solvents in which the metal carbonyls are at least slightly soluble. Treatment of 1 equiv of $Cp_2Ta(CH_2)(CH_3)$ (**1**) with 1 equiv of $Co_2(CO)_8$ or $Fe_2(CO)_9$ in tetrahydrofuran above −30 °C for 3 h results in >90% (^{1}H NMR) yields of dark brown and dark red compounds, respectively, with the stoichiometries $Cp_2Ta(CH_3)(C_3H_2O_2)Co_2(CO)_6$ (**17**) and $Cp_2Ta(CH_3)(C_3H_2O_2)Fe_2(CO)_7$ (**18**) (eq 4). Crystals

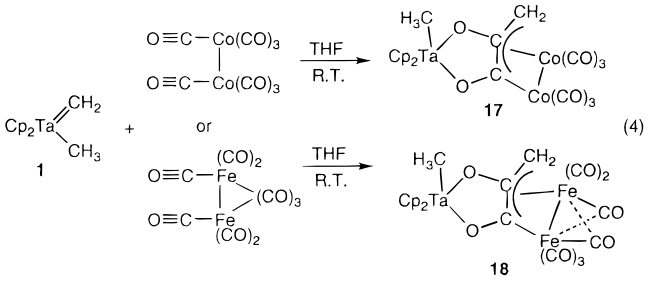

were isolated of compound **17** in 49% yield and compound **18** in 47% yield by slow diffusion of pentane into a benzene solution of the filtered reaction mixture. The ^{1}H NMR spectra of **17** and **18** are similar and suggest the formation of an unusual oxoallylidene structure bridging the three metal centers. The spectra of each show two inequivalent Cp resonances at δ 5.23 and 5.09 ppm (for **17**) and a tantalum methyl resonance. The two coupled inequivalent doublets (at δ 3.12 and 2.49 ppm) in the correct region for late-metal bound allylic protons suggested the presence of an allylic group.[21] The methylidene fragment is no longer bound to the quadrupolar tantalum center as shown by the large upfield shift and increased sharpness of the methylene resonances. The $^{13}C\{^1H\}$ NMR spectra of **17** and **18** are also quite similar with three resonances attributable to allylic carbons, two Cp resonances, a $Ta-CH_3$ resonance, and

(18) The zwitterion appears to be stable with respect to addition of more **1**.

(19) van Asselt, A.; Trimmer, M. S.; Henling, L. M.; Bercaw, J. E. *J. Am. Chem. Soc.* **1988**, *110*, 8254.

(20) Parkin, G.; van Asselt, A.; Leahy, D. J.; Whinnery, L.; Hua, N. G.; Quan, R. W.; Henling, L. M.; Schaefer, W. P.; Santarsiero, B. D.; Bercaw, J. E. *Inorg. Chem.* **1992**, *31*, 82.

(21) Collman, J. P.; Hegedus, L. S.; Norton, J. R.; Finke, R. G. *Principles and Applications of Organotransition Metal Chemistry*; University Science Books: Mill Valley, CA, 1987.

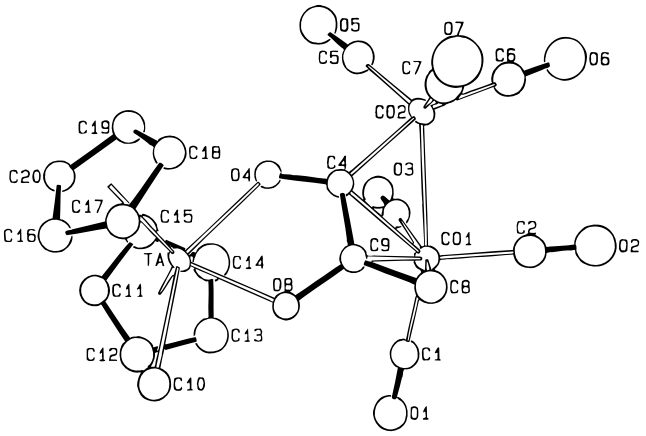

Figure 3. ORTEP diagram of $Cp_2Ta(CH_3)(\mu\text{-}C_3H_2O_2)Co_2(CO)_6$ (**17**).

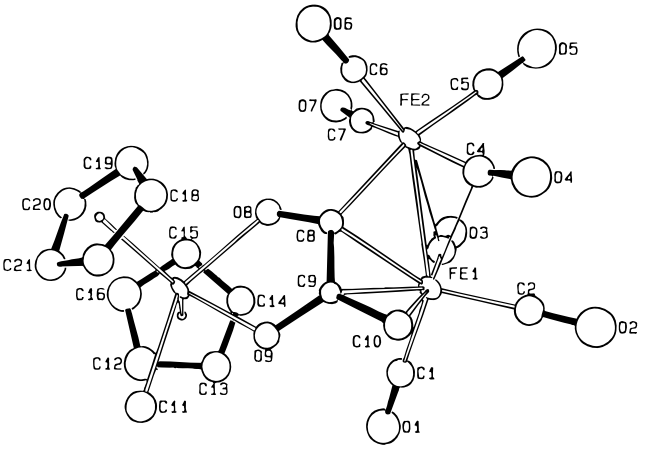

Figure 4. ORTEP diagram of $Cp_2Ta(CH_3)(\mu\text{-}C_3H_2O_2)Fe_2(CO)_7$ (**18**).

M−C≡O resonances. The $TaFe_2$ complex **18** does, however, have quaternary ^{13}C resonances (e.g. δ 144.4 ppm) which are indicative of semibridging carbonyls,[22] and the $TaCo_2$ complex **17** does not. The large differences between the chemical shifts of the allylic carbon resonances suggest that each of the carbons are in unique chemical and magnetic environments. Infrared data also show that along with numerous terminal C≡O stretches, absorbances for C−O single bonds also are observed.

The structures of **17** and **18** were established by single-crystal X-ray diffraction analyses (Figures 3 and 4, Tables 3 and 4). The bridging $C_3H_2O_2$ unit is bound to the Ta center through two Ta−O single bonds and is associated with one late metal center in an allylic type fashion with all three carbons of the ligand. The second late metal center is bound to only a single C atom of this ligand.[23] The different magnetic and chemical environments of each of the carbon atoms are apparent from the structure. One of the late metal centers sits significantly below the nearly planar dioxoallylic group accounting for the inequivalent Ta−Cp NMR resonances. The tantalum−methyl bond is retained but the CH_2 group is no longer associated with the tantalum center.

Reaction of $(\eta^5\text{-}C_5H_5)_2Ta(CH_2)(CH_3)$ with the Metal Carbonyls $Re_2(CO)_{10}$, $Mn_2(CO)_{10}$, and $Fe(CO)_5$. In contrast to the 1:1 stoichiometry of the reaction of **1** with the dicobalt and diiron carbonyls, the dirhenium and dimanganese carbonyls (which have M−M bond lengths of >2.8 Å), as well as $Fe(CO)_5$, react rapidly at room temperature with 2 equiv of $Cp_2Ta(CH_2)(CH_3)$. After 1 h at $T \geq 5$ °C, compounds with the stoichiometry $Cp_2(CH_3)Ta(C_3H_3)(CO)Re_2(CO)_8$ (**19**), $Cp_2(CH_3)Ta(C_3H_3)(CO)Mn_2(CO)_8$ (**20**), and $Cp_2(CH_3)Ta(C_3H_3)(CO)Fe(CO)_3$ (**21**) result (eq 5). These deep red compounds are isolated in crystalline form in good yield (62%, 58%, and 47% for **19**, **20**, and **21**, respectively, based on the metal carbonyls) upon pentane diffusion into a benzene or toluene solution of product

Table 3. Selected Intramolecular Distances and Angles for $Cp_2(CH_3)Ta(C_3H_2O_2)Co(CO)_6$ (**17**)

	Distance (Å)		
Ta−O4	2.150(7)	Co1−C4	2.233(11)
Ta−O8	2.074(7)	Co1−C8	2.105(12)
Ta−C10	2.278(12)	Co1−C9	2.151(11)
		Co2−C4	1.904(11)
Co1−Co2	2.573(2)		
		C4−O4	1.308(13)
		C9−O8	1.361(13)
		C4−C9	1.459(15)
		C8−C9	1.398(16)
	Angle (deg)		
O4−Ta−O8	72.7(3)	Co2−C4−O4	125.7(8)
O4−Ta−C10	143.2(4)	Co2−C4−C9	122.2(8)
O8−Ta−C10	70.5(4)		
		O4−C4−C9	112.1(9)
Co2−Co1−C4	46.0(3)	O8−C9−C4	114.0(9)
Co2−Co1−C8	87.9(3)	O8−C9−C8	122.8(10)
Co2−Co1−C9	76.8(3)	C4−C9−C8	122.8(10)
Co1−Co2−C4	57.5(3)		
Ta−O4−C4	120.7(7)	Co1−C4−Co2	76.4(4)
Ta−O8−C9	120.1(6)	Co1−C4−O4	129.5(8)
		Co1−C9−O8	125.7(8)

Table 4. Selected Intramolecular Distances and Angles for $Cp_2(CH_3)Ta(C_3H_2O_2)Fe_2(CO)_7$ (**18**)

	Distance (Å)		
Ta−O8	2.107(8)	C8−O8	1.311(13)
Ta−O9	2.073(7)	C9−O9	1.341(13)
Ta−C11	2.291(12)	C8−C9	1.426(15)
		C9−C10	1.419(15)
Fe1−Fe2	2.648(2)		
		Fe1−C3	1.771(12)
Fe1−C8	2.177(11)	Fe2−C4	1.800(12)
Fe1−C9	2.192(10)	Fe2−C3	2.873(12)
Fe1−C10	2.143(12)	Fe1−C4	2.671(12)
Fe2−C8	2.001(11)	C3−O3	1.150(14)
		C4−O4	1.148(14)
	Angle (deg)		
O8−Ta−O9	71.9(3)	Fe2−Fe1−C3	78.4(4)
O8−Ta−C11	142.6(4)	Fe2−Fe1−C8	47.8(3)
O9−Ta−C11	70.7(4)	Fe2−Fe1−C9	79.3(3)
		Fe2−Fe1−C10	94.1(3)
Fe1−C8−O8	132.6(8)	Fe1−Fe2−C4	70.9(4)
Fe2−C8−O8	118.1(8)	Fe1−Fe2−C8	53.7(3)
Fe1−C9−O9	127.2(7)	C4−Fe2−C8	96.9(5)
Fe1−C8−Fe2	78.5(4)	Fe1−C3−O3	174.9(11)
Fe2−C8−C9	129.4(8)	Fe2−C4−O4	166.2(11)
O8−C8−C9	112.2(9)		
O9−C9−C8	113.2(9)		
O9−C9−C10	121.7(9)		
C8−C9−C10	124.1(10)		

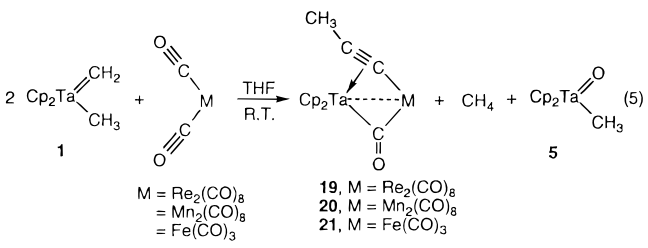

(22) Cotton, F. A. *Prog. Inorg. Chem.* **1976**, *21*, 1.

(23) Phosphine-substituted uranium carbene complexes have been shown to undergo a similar reaction with dinuclear iron carbonyls; compare with: Gilje, J. W.; Cramer, R. E. *Inorg. Chim. Acta* **1987**, *139*, 177.

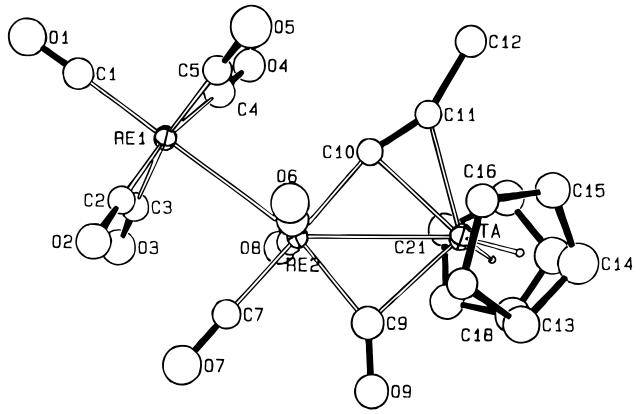

Figure 5. ORTEP diagram of $Cp_2(CH_3)Ta(\mu\text{-}C_3H_3)(CO)Re_2(CO)_8$ (**19**).

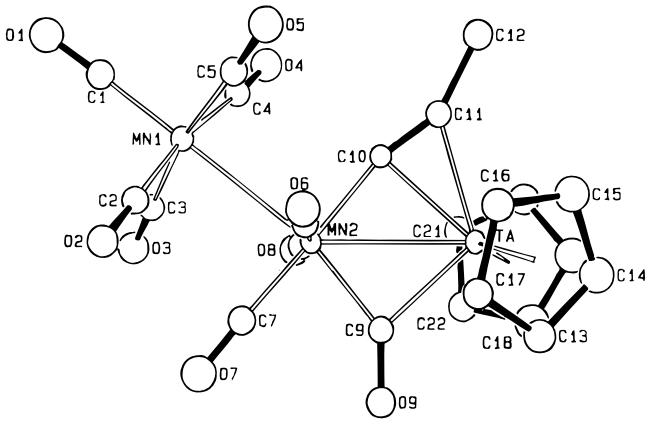

Figure 6. ORTEP diagram of $Cp_2(CH_3)Ta(\mu\text{-}C_3H_3)(\mu\text{-}CO)Mn_2(CO)_8$ (**20**).

followed by slow cooling to −40 °C. Also formed in these reactions are 1 equiv of $Cp_2Ta(=O)(CH_3)$ (**5**) and CH_4. The polynuclear products formed contain a bridging carbonyl and an unusual methylacetylide ligand, both of which bridge the tantalum and a single late-metal center.

The ^{1}H NMR spectra of **19**, **20**, and **21** are all similar and straightforward. Only two resonances occur in each, the equivalent Cp rings of the tantalum and a methyl group in the proper region for a bound methylacetylide ligand (δ 3.01 ppm for **19**). The ^{13}C NMR spectrum of these show resonances attributable to two quaternary and one primary carbon (in addition to those associated with CO and Cp ligands). The chemical shift and the sharpness of the methyl ^{13}C and ^{1}H resonances (δ 3.01 ppm in ^{1}H NMR for **19**) suggest the idea that it is no longer bound directly to the tantalum center. Also, a downfield CO resonance is observed in each of the spectra (δ 266.5 ppm in ^{13}C NMR for **19**) and an IR ν_{CO} stretching absorption at around 1713 cm^{-1} (for **19**) suggests that there is an unusual bridging carbonyl ligand between the tantalum and a late metal center.

Once again X-ray diffraction was used to conclusively establish the structures of **19, 20**, and **21** (Figures 5−7; Tables 5−7). The molecular geometry revealed conclusively the multinuclear structures in which the early and late metal centers are bridged by both a CO ligand and a three-carbon methylacetylide ligand. Interestingly, these structures are also the first examples of bridging carbonyls attached to Ta.

The general geometry about the $Ta(C_3H_3)(CO)M$ fragment has allowed us to determine some bonding distances that have thus far been absent from the literature. The Ta−M distances seem to vary directly with respect to the size of the late-metal radii: the Ta−Fe bonding distance is 2.880(1) Å, Ta−Mn is 2.931(1) Å, and Ta−Re is 3.017(1) Å. The bridging C=O bond distance does not change significantly from metal to metal indicating that there is no systematic change in electron donation from the two metal centers into the CO antibonding orbitals.

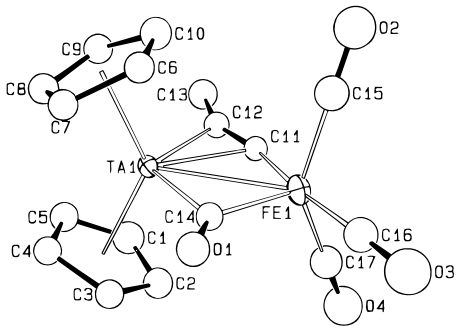

Figure 7. ORTEP diagram of one of the two crystallographically independent molecules of $[Cp_2(CH_3)Ta(\mu\text{-}C_3H_3)(\mu\text{-}CO)Fe(CO)_3]_2\cdot(C_6H_6)$ (**21**).

Table 5. Selected Intramolecular Distances and Angles for $Cp_2Ta(C_3H_3)(CO)Re_2(CO)_8$ (**19**)

	Distance (Å)		
Re1−Re2	3.001(1)	Ta−C9	2.313(21)
Re2−Ta	3.017(1)	Ta−C10	2.283(19)
		Ta−C11	2.289(18)
Re2−C9	2.018(22)		
Re2−C10	2.029(18)	C9−09	1.216(23)
		C10−C11	1.28(3)
		C11−C12	1.52(3)
	Angle (deg)		
Re2−C10−Ta	88.6(7)	C9−Ta−C10	84.2(7)
Re2−C10−C11	162.1(16)	C9−Ta−C11	116.4(7)
C10−C11−C12	152.4(20)	Re2−C9−O9	143.4(17)
Ta−C11−C12	134.0(14)	Ta−C9−O9	128.3(16)
		Re2−C9−Ta	88.0(8)
Re1−Re2−Ta	144.37(3)		
Re1−Re2−C9	165.0(6)		
Re1−Re2−C10	95.3(5)		
C9−Re2−C10	99.1(8)		

Table 6. Selected Intramolecular Distances and Angles for $Cp_2Ta(C_3H_3)(CO)Mn_2(CO)_8$ (**20**)

	Distance (Å)		
Ta−Mn2	2.931(l)	C10−C11	1.259(10)
Mn2−Mn1	2.880(2)	C11−C12	1.492(11)
Ta−C9	2.251(7)		
Ta−C10	2.243(7)	C9−O9	1.211(8)
Ta−C11	2.280(7)		
Mn2−C9	1.931(7)		
Mn2−C10	1.921(7)		
	Angle (deg)		
C9−Ta−C10	82.1(3)	Mn2−C10−Ta	89.1(3)
Ta−Mn2−Mn1	142.39(4)	Mn2−C10−C11	164.1(6)
		C10−C11−C12	151.9(8)
Ta−C9−O9	131.5(6)	Ta−C11−C12	135.7(6)
Mn2−C9−O9	139.8(6)		
Mn2−C9−Ta	88.6(3)	Mn1−Mn2−C9	167.3(2)
		Mn1−Mn2−C10	92.5(2)

In order to determine whether the carbon atoms in the C_3H_3 ligand originate from the tantalum complex or from carbon monoxide, the labeled tantalum methylidene complex ($Cp_2Ta(^{13}CH_2)(^{13}CH_3)$ (**1-$^{13}C_2$**)) was allowed to react with $Re_2(CO)_{10}$. The resulting $Re-{}^{12}C\equiv{}^{13}C-{}^{13}CH_3$ labeling pattern demonstrated conclusively that the β-carbon and methyl carbon of the acetylide ligand came from the tantalum center and not from a carbonyl ligand. Also, the $^{13}CH_4$ and oxotantalum complex **5** generated concurrently with **19** contained a single ^{13}C label each.

Table 7. Selected Intramolecular Distances and Angles for One of the Two Crystallographically Independent Molecules of $[Cp_2Ta(C_3H_3)(CO)Fe(CO)_3]_2\cdot(C_6H_6)$ (**21**)

	Distance (Å)		
Ta1−Fe1	2.880(1)	Fe1−C11	1.881(10)
		Fe1−C14	1.935(11)
Ta1−C11	2.248(10)		
Ta1−C12	2.307(11)	C11−C12	1.258(14)
Ta1−C14	2.234(10)	C12−C13	1.500(16)
		C14−O1	1.193(12)
	Angle (deg)		
C14−Ta1−C11	82.9(4)	Fe1−C11−C12	164.3
C14−Ta1−C12	114.9(4)	Fe1−C11−Ta1	88.0(4)
		C11−C12−C13	153.8(11)
C11−Fe1−C14	102.0(4)	Ta1−C12−C13	134.8(8)
		Ta1−C14−Fe1	87.1(4)
		Ta1−C14−O1	136.2(8)
		Fe−C14−O1	136.7(8)

In another labeling experiment, the ^{13}C-enriched alkylidene complex, $Cp_2Ta(^{13}CH_2)(CH_3)$ (**1-^{13}C**), was prepared by photolysis of the ethylene complex, $Cp_2Ta(C_2H_4)(CH_3)$, in the presence of $(C_6H_5)_3P{=}{}^{13}CH_2$. This labeled alkylidene complex did not show any significant scrambling to the methyl position (<5% by NMR) over the course of 3 h at room temperature. Metal carbonyl ($Re_2(CO)_{10}$ or $Fe(CO)_5$) was added at low temperature in THF-d_8 to this mixture, and the sealed tube containing the mixture was inserted into a pre-cooled NMR probe. The progress of the reaction was then monitored by variable-temperature NMR. Unexpectedly, in the presence of the metal carbonyl, there was rapid prescrambling of the ^{13}C label in **1-^{13}C** (eq 6). Subsequent reaction of label-scrambled

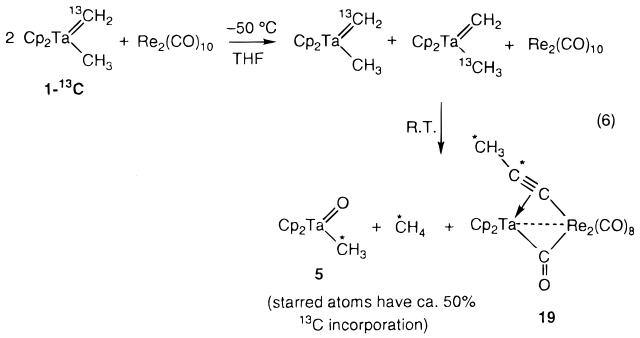

(6)

1 with the metal carbonyl gave product having a statistical mixture of the labeled carbon in the β and γ positions of the methyl acetylide ligand, in the methyl group of $Cp_2Ta(=O)(CH_3)$, and in the methane produced. There was no (<5% by NMR) labeled ^{13}C in the α-position of the methyl acetylide ligand of the product. The mechanism of the rapid rhenium-catalyzed pre-scrambling is unclear. A further control experiment was performed to show the origin of the α-carbon of the acetylide ligand. Labeled $Re_2(^{13}CO)_{10}$ was allowed to react with **1**, and analysis of the final products showed ^{13}C label in only the Re-bound carbons, including the α-carbon of the acetylide ligand ($[Re]-{}^{13}C{\equiv}C-CH_3$).

By performing variable-temperature NMR experiments during the reaction of **1** and $Re_2(CO)_{10}$, we were able to observe the formation of unstable intermediates which have been characterized by ^1H NMR. A sealed NMR tube containing a THF-d_8 solution of **1** and $Re_2(CO)_{10}$[24] at −78 °C was inserted into a pre-cooled probe. Upon slow warming of the reaction mixture, a new material was formed whose spectral characteristics were consistent with its assignment as zwitterion **22** (eq 7). On reaching 5 °C, a second equivalent of **1** was consumed, concurrent with the formation of CH_4 and 1 equiv of $Cp_2(CH_3)Ta{=}O$ (**5**) to give the isolable product **19**.

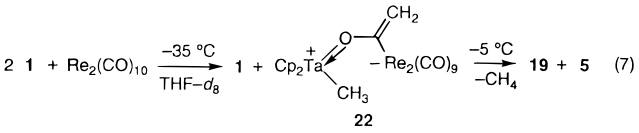

(7)

In these structures in which acetylide and carbonyl ligands bridge the two metal centers, there is some question as to the presence or absence of an early metal−late metal bond. Part of this has to do with the presence of a bent semibridging carbonyl, a geometry in which the carbonyl is associated much more closely with the late metal center than with the tantalum. A widely accepted rationale[25] for the nature of semibridging carbonyls would suggest that the carbonyl accepts electron density from the Ta center into its 2π orbital thus stabilizing the charge difference between the two metals.[22,26] However, the presence of a semibridging carbonyl does not necessarily signify strong metal-to-metal binding, so the presence of a metal−metal bond must be rationalized further on electronic bases. In the case of the TaFe complex (**21**) we consider the oxidation states as Ta(III)[27] and Fe(II); the number of valence electrons around the Fe(II) center (ignoring the presence of a metal−metal bond) is 16. Donation of two d electrons from the Ta(III) center to the Fe center would bring the total electron count on Fe to 18. The Ta−Fe distance of 2.880 Å does not rule out this kind of interaction. Little is known about Ta−Fe, −Mn, or −Re interactions. In the only structurally characterized case which contains one of these bonds (a Ta−Mn bond), the literature claims a Ta−Mn bonding distance of 3.441(1)Å.[28] This compares with the TaMn distance in **20** of 2.931(1) Å. We conclude that there is significant metal−metal overlap in **20**.

Reaction of $Cp_2Ta(CH_2)(CH_3)$ with the Trinuclear Metal Carbonyl Cluster $Ru_3(CO)_{12}$. Treatment of a THF slurry of ($Ru_3(CO)_{12}$) with 2 equiv of the tantalum alkylidene complex $Cp_2Ta(CH_2)(CH_3)$ (**1**) at temperatures greater than 5 °C results in the formation of 1 equiv of the previously characterized oxo complex, $Cp_2Ta(=O)(CH_3)$ (**5**), and a $TaRu_3$-containing cluster complex, **23** (eq 8). Monitoring this reaction by NMR

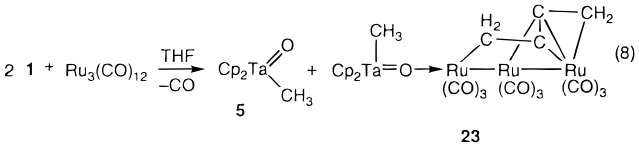

(8)

demonstrated that this species was formed in 57% yield (based on ^1H NMR). Recrystallization from benzene/pentane by vapor

(24) Due to the lack of solubility of $Re_2(CO)_{10}$ at −78 °C, the mixture was heterogeneous during the initial stages of the reaction.

(25) Jemmis, E. D.; Pinhas, A. R.; Hoffmann, R. *J. Am. Chem. Soc.* **1980**, *102*, 2576.

(26) It is also possible that the difference in geometry concerning the metal−carbonyl bond lengths can be attributed to the difference in metal orbital character between the early- and late-metal centers; see: Simpson, C. Q.; Hall, M. B. *J. Am. Chem. Soc.* **1992**, *114*, 1641 and references cited therein.

(27) The formal oxidation state (Ta(III) vs Ta(V)) is unclear because the bridging propyne ligand is neither linear (an argument for a Ta(III) center) nor bent to the extent of a normal alkene (the Ta−C−C angle in **20** is 151.9(8)°) which would lead to a cyclopropene-like Ta(V) structure. We believe that there is at least a significant contribution from the Ta(III) resonance form.

(28) Balbach, B.; Baral, S.; Biersack, H.; Hermann, W. A.; Labinger, J. A.; Scheidt, W. R.; Timmers, F. J.; Ziegler, M. L. *Organometallics* **1988**, *7*, 325.

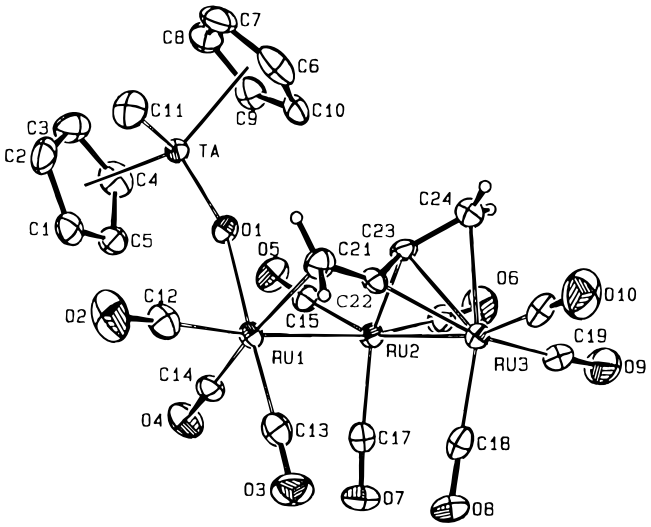

Figure 8. ORTEP diagram of $Cp_2(CH_3)Ta(\mu\text{-}O)Ru_3(\mu\text{-}\eta^1{:}\eta^1{:}\eta^3\text{-}C_4H_4)(CO)_9$ (**23**).

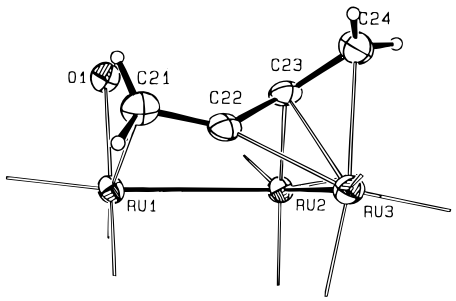

Figure 9. ORTEP diagram of the $ORu_3(C_4H_4)$ fragment of **23**.

diffusion provided analytically pure **3** as yellow crystals in 32% isolated yield.

The mass spectrum of **23** showed a parent ion at $[M^+] = 950.8$ *m/z*, and the fragmentation pattern was consistent with a general formula of $Cp_2(CH_3)Ta(O)Ru_3(C_4H_4)(CO)_9$. A C_6D_6 solution of **23** shows a methyl singlet at δ 0.35 ppm, a singlet for each of two inequivalent cyclopentadienyl groups at δ 5.10 and 5.17 ppm, and signals for four inequivalent methylene protons. One set of methylene doublets appearing at δ 4.39 and 4.26 ppm are coupled to each other with $^2J_{HH} = 2.6$ Hz while a second set of doublets at δ 2.00 and 1.51 ppm have a coupling constant $^2J_{HH} = 1.3$ Hz. The ^{13}C NMR spectrum with DEPT analysis showed (in addition to the carbonyl resonances) the presence of two methylene carbons and two quaternary carbons and characteristic resonances for the $Cp_2(CH_3)$-Ta(=O) bridging oxo species. Our initial assignment of the species as a triruthenium cluster core, to which are bound a $Cp_2(CH_3)Ta{=}O$ fragment and a butadiene or [3]-cumulene ($H_2C{=}C{=}C{=}CH_2$) ligand, was based on its similarity to the allylic species described above in the reactions of **1** with the $Co_2(CO)_8$ and $Fe_2(CO)_9$ clusters. A single-crystal X-ray diffraction analysis was undertaken at −83 °C to confirm our initial hypothesis. In the solid state, the structure consists of two crystallographically related molecules of **23** and one molecule of benzene in the triclinic unit cell. The hydrogen atoms, including the methylene hydrogens on the C_4H_4 ligand, were located in difference Fourier maps and allowed to refine with isotropic thermal parameters (Figures 8 and 9; Tables 8 and 9).

Within the cluster, the $Cp_2(CH_3)Ta{=}O$ moiety bound to one end of the Ru_3 chain appears to simply fill one of the coordination sites left vacant by loss of a CO ligand at the Ru_1 center, a situation that is superficially similar to that observed in the $Cp_2(CH_3)Ta(=O)-Re(C(=CH_2)Ph)(CO)_4$ (**3b**) complex

Table 8. Selected Intramolecular Distances for $Cp_2(CH_3)Ta(O)Ru_3(C_4H_4)(CO)_9{\cdot}0.5C_6H_6$ (**23**)

	Distance (Å)		
Ru1−Ru2	2.942(1)	Ru1−O1	2.102(3)
Ru2−Ru3	2.767(1)	Ru1−C12	1.953(5)
		Ru1−C13	1.853(5)
Ru1−C21	2.216(5)	Ru1−C14	1.927(6)
Ru2−C23	2.043(5)	Ru2−C15	1.897(5)
Ru3−C22	2.132(5)	Ru2−C16	1.883(5)
Ru3−C23	2.156(4)	Ru2−C17	1.930(5)
Ru3−C24	2.289(5)	Ru3−C18	1.894(5)
		Ru3−C19	1.932(6)
C21−C22	1.366(7)	Ru3−C20	1.934(6)
C22−C23	1.410(7)		
C23−C24	1.391(7)	Ta−O1	1.791(3)
		Ta−C11	2.205(6)
		Ta−CP1	2.138
		Ta−CP2	2.146

Table 9. Selected Intramolecular Angles for $Cp_2(CH_3)Ta(O)Ru_3(C_4H_4)(CO)_9{\cdot}0.5(C_6H_6)$ (**23**)

	Angle (deg)		
Ru2−Ru1−O1	86.71(9)	Ru1−C21−C22	82.4(3)
Ru2−Ru1−C21	89.74(14)	Ru1−C21−H21A	106.6(26)
O1−Ru1−C21	84.07(17)	Ru1−C21−H21B	100.4(34)
C12−Ru1−C21	86.12(21)	C22−C21−H21A	114.8(25)
C13−Ru1−C21	92.48(22)	C22−C21−H21B	117.4(34)
C14−Ru1−C21	169.65(20)	H21A−C21−H21B	123.5(43)
		Ru3−C22−C21	145.3(4)
Ru1−Ru2−Ru3	91.33(2)	C21−C22−C23	140.2(5)
		Ru2−C23−Ru3	82.37(16)
RU1−Ru2−C23	78.60(14)	Ru2−C23−C22	95.1(3)
Ru3−Ru2−C23	50.58(12)	Ru2−C23−C24	129.8(4)
C15−Ru2−C23	107.40(20)	C22−C23−C24	118.9(5)
C16−Ru2−C23	93.02(22)	Ru3−C24−C23	66.6(3)
C17−Ru2−C23	148.66(20)	Ru3−C24−H24A	111.3(34)
		Ru3−C24−H24B	99.0(30)
Ru2−Ru3−C22	62.08(13)	C23−C24−H24A	116.2(36)
Ru2−Ru3−C23	47.05(13)	C23−C24−H24B	118.3(32)
Ru2−Ru3−C24	75.62(15)	H24A−C24−H24B	124.6(48)
C22−Ru3−C24	66.00(19)		
		Ta−O1−Rul	162.85(18)
		CP1−Ta−CP2	129.78
		O1−Ta−C11	94.23(20)

reported above. However, the Ta(=O)−Ru bonding in the two complexes appears to be different. In the Ta(=O)−Re case, the angle between the three atoms is essentially linear (179.0-(6)°), whereas the Ta(=O)−Ru angle in **23** is 162.8(2)°. We do not know whether this difference is caused by electronic or steric factors.

As expected for third-row metals,[29] the CO's in this structure are not bridging as was observed in the $TaFe_2$ cluster described above. There are also two apparent Ru−Ru bonds, from Ru_1 to Ru_2 (2.942(1) Å) and from Ru_2 to Ru_3 (2.767(1) Å). The Ru−Ru−Ru angle is 91.3°, indicating that there is no third Ru_1−Ru_3 bond (ca. 4.1 Å). The longer Ru_1−Ru_2 interaction may or may not correspond to a full single bond. Distances ranging from 2.64 to 3.16 Å have been found in 140 other ruthenium cluster structures that contain a Ru−Ru−Ru fragment. Distances at the higher end of this range (>3.1 Å) are probably too long to be conventional two-electron covalent bonds and most likely represent bridging structures that do not require a large degree of metal−metal interaction. Each Ru center is approximately octahedrally coordinated. The pseudo-octahedron of Ru1 is tilted about 45° with respect to the pseudo-octahedra

(29) Ru carbonyl clusters typically have fewer bridging carbonyls when compared to the analogous Fe clusters. For example, see: Churchill, M. R.; Hollander, F. J.; Hutchinson, J. P. *Inorg. Chem.* **1977**, *16*, 2655.

Scheme 2

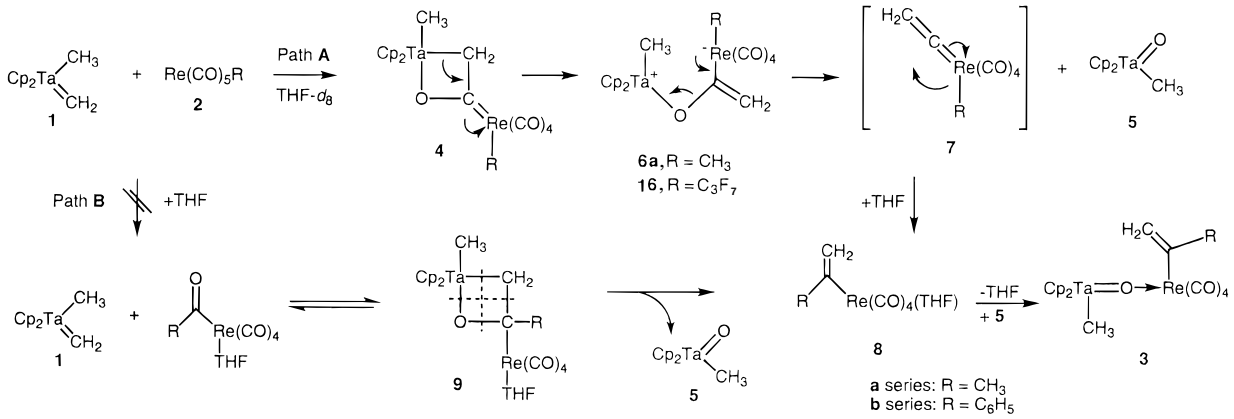

of Ru_2 and Ru_3, and the latter are approximately parallel to each other. There are no apparent systematic differences in the Ru−C distances or Ru−O distances to the carbonyl ligands.

"Above" the Ru_3 plane lies a twisted non-cyclic ligand of composition C_4H_4. The hydrogen atoms at each terminus were located and refined. Each carbon atom of the ligand coordinates to at least one Ru atom, and C_{23} bridges the Ru_2-Ru_3 bond. The Ru−C distances vary from 2.043(5) to 2.289(5) Å with the longest distance being Ru_3-C_{24}. The C−C distances and angles and C−C−C−C torsion angle are not consistent with any obvious simple bonding scheme. The hybridization at C_{21} appears to be essentially sp^2, with a somewhat lengthened C═C double bond, but this atom is also bonded to Ru_1 with a C═C−Ru angle of 82.4(3)° and a C−C−C−Ru torsion angle of 92.41(68)°. The hydrogen atoms are located nearly in the C−C−C plane, with both displaced slightly away from the coordinated Ru.

The bonding at C_{22} and C_{23} is more complex. The C−C−C angle of 140.2(5)° at C_{22} is reasonable for two coordinated sp-hybridized carbons, such as those found in complexed alkynes, but the angle at C_{23} (118.9(5)°) is more typical of a relatively undistorted sp^2 carbon. Ru_3 is in the $C_{21}-C_{22}-C_{23}$ plane, but the coordination is more consistent with that of a C═C double bond, with both C_{22} and C_{23} at essentially the same distance from Ru_3 and with the C−C distance lengthened to 1.410(7) Å. In addition, there is an obvious Ru−C single bond from Ru_2 to C_{23}, but Ru_2 lies out of the plane of $C_{21}-C_{22}-C_{23}$ by 1.81 Å (and out of the $C_{22}-C_{23}-C_{24}$ plane by 1.26 Å).

This is further complicated by a twisting of the C_4 ligand, leading to a C−C−C−C torsion angle of 101.3(7)°. This twist clearly excludes the possibility of an undistorted cumulene structure. Instead, Ru_3 coordinates to three of the carbons in what at first appears to be an allylic-type bonding arrangement with respect to the $C_{22}-C_{23}-C_{24}$ plane. The $C_{23}-C_{24}$ distance of 1.391(7) Å reflects a typically allylic bond order of approximately 1.5, but the bonding distance to C_{24} is much longer than the distances to C_{22} and C_{23}, making even this interaction highly unsymmetrical. In addition, the hydrogen atom positions on C_{24} are twisted with respect to the C_{21}-C_{22}-C_{23} plane so as to give them more equivalent Ru−C−H angles.

With these unusual positional parameters in mind, a formal bonding scheme is still difficult to formulate. However, a somewhat distorted allylic-type interaction, as discussed later and illustrated in Scheme 6, is the simplest formulation of the bonding between $C_{22}-C_{23}-C_{24}$ and the Ru_3 core. With a $C_{23}-Ru_2$ single bond, the only bonding assignments left are those between C_{21}, C_{22}, and Ru_1. If the 1.366(7) Å distance between C_{21} and C_{22} is a somewhat lengthened double bond, then one must consider whether there is any significant $C_{22}-Ru_1$ bonding. This is difficult to say decisively, but we have not found any clear evidence for a Ru−C bonding distance of greater than 2.35 Å. Thus our formulation does not include a bond between these two atoms. Because it seems clear that the sp^2 carbon is in the proper arrangement for it, we postulate a donor coordination from C_{21} to Ru_1.

Discussion

The metal carbonyls that react with $Cp_2Ta(CH_2)(CH_3)$ span groups 7, 8, and 9 of the periodic table, include 3d, 4d, and 5d metal centers, can be monomeric, dimeric or trimeric metal complexes, and in some cases have alkyl, aryl, or vinyl groups attached to the late metal center. As a result, an unusually wide range of structural types are formed as products in these reactions. However, in the initial stages these reactions appear to proceed similarly despite any difference in the metal centers involved.

In the reaction of **1** with substituted rhenium carbonyls, the two most likely mechanisms, illustrated in Scheme 2, differ in the relative timing of the migratory insertion and CO deoxygenation steps that must occur in the conversion of **2** to **3**. Another mechanism, which is not shown, involves preliminary CO loss from the Re center. However, it is unlikely that the reaction proceeds by an initial loss of CO from Re because such dissociation normally requires light or relatively high temperatures.[30] A more likely mechanism (path A in Scheme 2) proceeds by "psuedo-Wittig-type" cyclization of the Ta═CH_2 moiety and a ReC≡O group, leading initially to oxametallacycle **4**. At this point, the reactive metallacycle undergoes rapid cleavage of the remaining Ta−CH_2 bond to yield a zwitterion (**6**) with an oxo−vinyl group (or formally a bridging ketene, μ-η^1:η^1-O═C═CH_2) connecting the early- and late-metal centers. This zwitterion is a thermally unstable species when the rhenium alkyl ligand is not perfluorinated, but was observed spectroscopically at low temperatures. Thermal fragmentation of the zwitterion (which cleaves the remaining carbon−oxygen bond) leads to the oxotantalum species **5** and the alkyl- or arylrhenium vinylidene complex **7**. The vinylidene complex then undergoes rapid solvent-induced migratory insertion to give THF solvate **8**. At this point, the solvent molecule is displaced by the tantalum oxo linkage in **5** to form the stable bridging oxo complex **3**.[16]

The second possible reaction pathway (path B in Scheme 2) involves initial migration of the alkyl or aryl group to a CO ligand. Subsequently, the tantalum alkylidene complex attacks the acyl species much as the Cp* (Cp* = η^5-C_5Me_5) analog of **1** has been shown to attack aldehydes (see intermediate **9**).[31]

(30) For example, see: Hieber, W.; Braun, W.; Beck, P. *Chem. Ber.* **1960**, *93*, 903.

Scheme 3

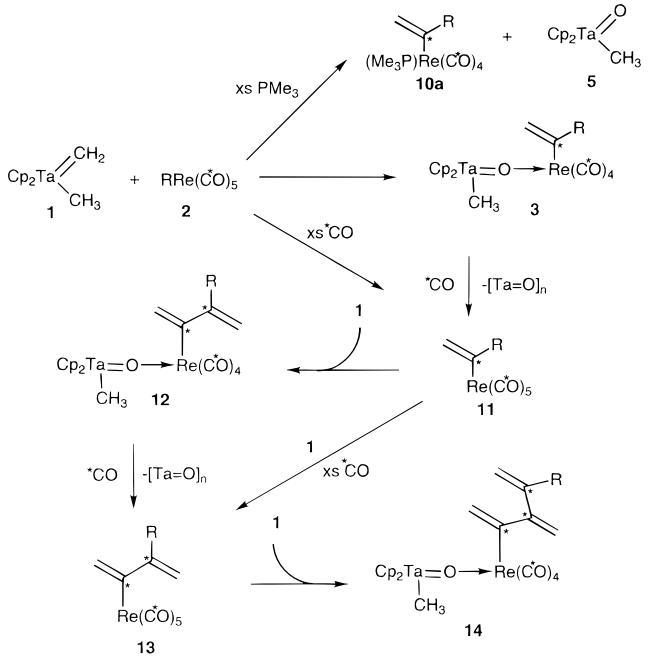

Scheme 4

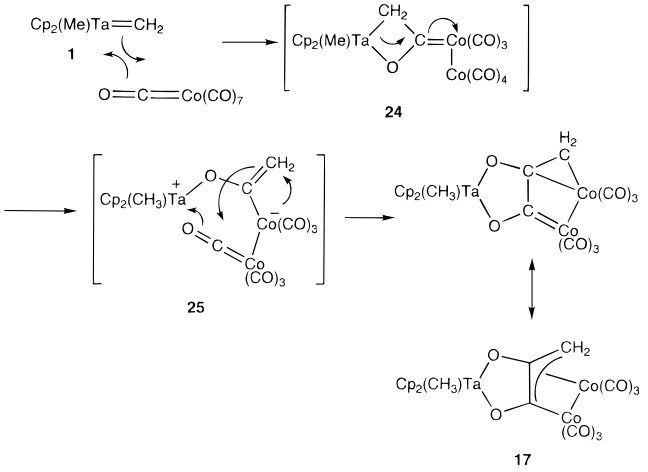

The isotope tracer and low-temperature NMR monitoring experiments allowed us to distinguish between these mechanistic alternatives. First, it was demonstrated that the vinyl methyl group arises essentially exclusively from the $Re(CH_3)$ rather than the $Cp_2Ta(CH_2)(CH_3)$ center. Because the proton resonance due to the rhenium methyl group in the first intermediate appears at δ −0.49 ppm, it is clear that it has not yet migrated away from the metal center. These observations are clearly more consistent with intermediate **6** in path A rather than intermediate **9** in path B.

In examining further the mechanism of the CH_2/O metathesis reaction that occurs between the tantalum methylidene complex **1** and the substituted rhenium pentacarbonyl complexes, we used the known stability of perfluorinated alkylrhenium complexes to isolate and characterize **16**. Because the ^{1}H NMR spectroscopic properties of the intermediate observed in the reaction of **1** with $MeRe(CO)_5$ (**2a**) are analogous to those of the structurally characterized perfluorinated zwitterionic species[6] **16** (Scheme 2), we believe that intermediate **6** has a similar zwitterionic character. We attribute the stability of this zwitterion (relative to the unsubstituted or hydrocarbon-substituted rhenium carbonyls) to the ability of the strongly-electron withdrawing perfluoroalkyl group to stabilize the negative charge that is apparently localized on the rhenium metal center.

In further support of pathway A, carrying out the low-temperature NMR-monitored reaction of **1** with **2a** in the presence of excess PMe_3 (Scheme 3) allowed us to trap $CH_3C(CH_2)Re(CO)_4(PMe_3)$ (**10a**) and see free $Cp_2(CH_3)Ta(=O)$ (**5**) produced in place of THF complex **8a** and bridging oxo complex **3a**. Similarly, trapped product $CH_3C(CH_2)Re(CO)_5$ (**11a**) is formed when excess CO was used in place of phosphine.

We were able to demonstrate the weakness of the tantalum oxo linkage by treating $Cp_2(CH_3)Ta{=}O{-}Re(CH_3C(CH_2))(CO)_4$ (**3a**) with carbon monoxide, which leads quickly to $CH_3C(CH_2)Re(CO)_5$ (**11a**) and $[Cp_2(CH_3)Ta{=}O]_n$. We continued this carbon chain growth by two more steps via deoxygenation of another carbonyl from **11a** (Scheme 3). We do not know how far this methylene-substituted chain can be extended, but it appears that growth of this unusual isomer of polyacetylene is driven by the tendency for the tantalum oxide to fall out of solution as a polymer and not build up in large concentration at room temperature.

Migratory insertion reactions of vinyl or alkyl vinylidene species have been documented recently,[13,14,32,33] but we believe the formation of **3b** is an unusual example of the much stronger metal aryl bond[21,34] undergoing migratory insertion with a vinylidene ligand to form an arylvinyl (α-styryl) complex. Also unusual are the rates of the migratory insertion reactions, which occur at temperatures below ambient.[35] To our knowledge conversion of **2** to **3** is the first observation of the "psuedo-Wittig type" sequence illustrated in Scheme 1, involving oxametallacycle and zwitterion formation from an alkylidene and metal-bound CO, followed by breakdown of the zwitterion intermediate to give a vinylidene product in which the carbon monoxide oxygen atom has been replaced with a CH_2 group.

Mechanism of Formation of $Cp_2Ta(CH_3)(O_2C_3H_2)M_2(CO)_x$ (17, M = Co, x = 6; 18, M = Fe, x = 7). Although we have collected somewhat less mechanistic information on the reaction of **1** with the dinuclear metal carbonyls $Fe_2(CO)_9$ and $Co_2(CO)_8$, our observations again point toward initial attack of the nucleophilic tantalum methylidene carbon on an electrophilic carbonyl carbon of the late metals.

In Scheme 4, a possible sequence is shown that we feel is the most likely pathway to the isolable complexes **17** and **18**. Both reactions are initiated by an overall cycloaddition between the $Ta{=}CH_2$ group of **1** and a CO ligand of the dinuclear metal carbonyl complex to give **24**. The ring in **24** rapidly opens by cleaving the tantalum−methylidene bond, at which point the reactive zwitterionic intermediate **25** is formed that contains a C_2H_2O ligand bridging the tantalum and a single late-metal center. This proposed intermediate is similar to the isolable intermediate **16** formed in the reaction of **1** with $C_3F_7Re(CO)_5$ in which carbon monoxide has inserted into the tantalum−methylidene double bond.

Following this initial reaction, we believe the second late-metal center of the iron or cobalt dinuclear carbonyl intermediate (**25**, Scheme 4) brings a second carbonyl into position to interact.

(31) Whinnery, L. L.; Henling, L. M.; Bercaw, J. E. *J. Am. Chem. Soc.* **1991**, *113*, 7575.

(32) Beevor, R. G.; Freeman, M. J.; Green, M.; Morton, C. E.; Orpen, A. G. *J. Chem. Soc., Chem. Commun.* **1985**, 68.

(33) Höhn, A.; Werner, H. *Organomet. Chem.* **1990**, *382*, 255.

(34) Group 7 metal−phenyl bonds have been reported to be about 5 kcal/mol stronger than group 7 metal−methyl bonds; see: Connor, J. A.; Zafarani-Moattar, M. T.; Bickerton, J.; El Saied, N. I.; Suradi, S.; Carson, R.; Al Takhin, G.; Skinner, H. A. *Organometallics* **1982**, *1*, 1166.

(35) In a related (alkyl)(aryl) rhenium complex, methyl migration has been reported to occur approximately 30 times faster than the corresponding phenyl group migration; see: Casey, C. P.; Scheck, D. M. *J. Am. Chem. Soc.* **1980**, *102*, 2723.

Scheme 5

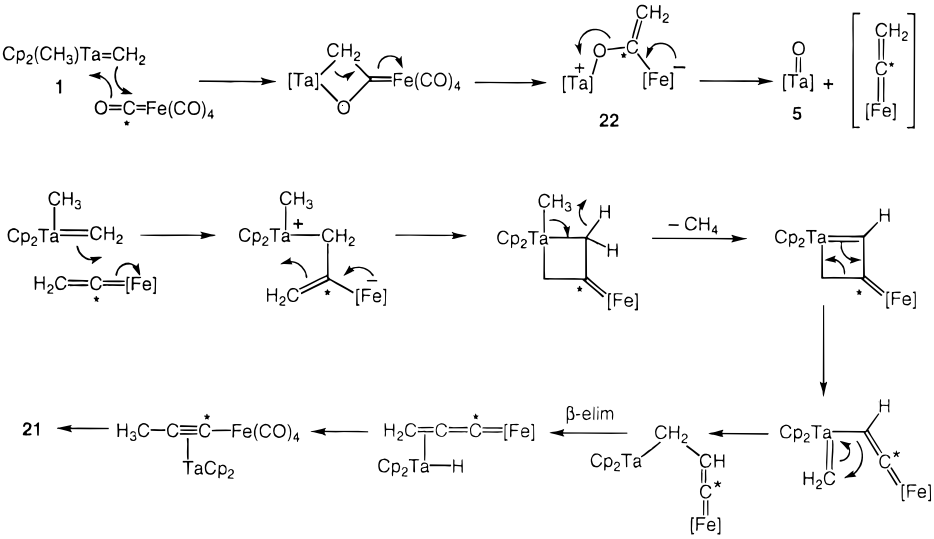

Scheme 6

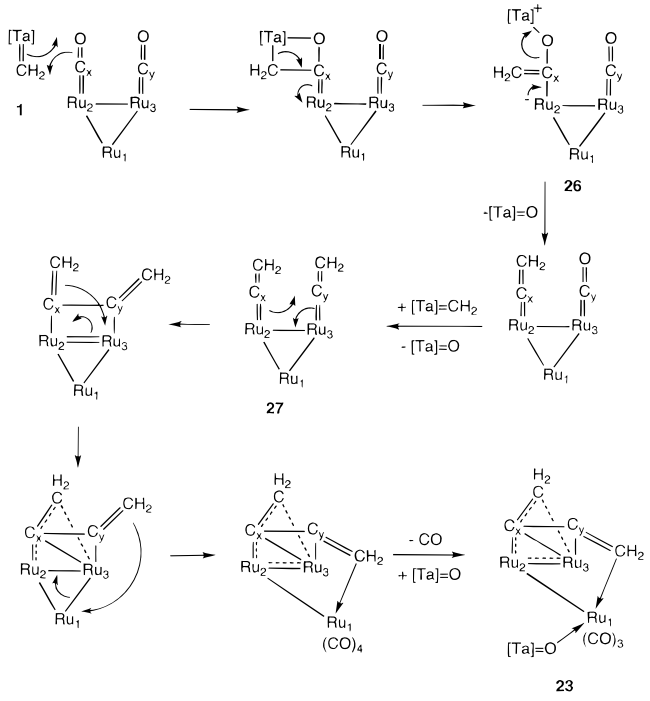

When a CO ligand moves into proximity, this group is attacked by the C_2H_2O ligand with the aid of the highly oxophilic and unsaturated (electronically *and* sterically) tantalum center. We believe the intramolecular attack of the second carbonyl is fast (relative to the initial intermolecular attack) because it must happen *before* the cleavage of the carbon−oxygen bond (as is seen in other systems described in this paper) and because we were unable to observe an intermediate during low-temperature reactions monitored by ^1H NMR.

Mechanism of Formation of $Cp_2Ta(\mu\text{-}C_3H_3)(\mu\text{-}CO)M_x(CO)_y$ (19, $M_x = Re_2$, $y = 8$; 20, $M_x = Mn_2$, $y = 8$; 21, $M_x =$ Fe, $y = 3$). The products formed in the reaction between **1** and $Re_2(CO)_{10}$, $Mn_2(CO)_{10}$, and $Fe(CO)_5$ offered a sharp contrast to those described above and therefore there must be significant mechanistic differences in these processes as well. It is difficult to understand how the extensive bonding changes occur that result in the formation of methylacetylide complexes **19**, **20**, and **21**. In Scheme 5, a mechanism is proposed that suggests at least one way this might happen (for brevity illustrated only for the Fe system). The spectroscopic and structural data discussed above support the first steps in which all reactions are initiated by an overall cycloaddition between the Ta═CH_2 group of **1** and a CO ligand of the metal carbonyls, and the oxametallacycle formed in this way then undergoes ring-opening to a thermally unstable zwitterionic intermediate that contains a C_2H_2O ligand bridging the tantalum and a single late-metal center. The Re_2, Mn_2, and Fe zwitterionic intermediates apparently do not allow a second carbonyl ligand into a close enough orientation to interact productively like the Co_2 and Fe_2 intermediates described above. Steric effects must play an important role in differentiating these two unique pathways, especially if one considers the electronic properties of the iron centers in $Fe(CO)_5$ and $Fe_2(CO)_9$ to be relatively similar.

After its formation the thermally unstable zwitterion **22** reacts at 25 °C with another equivalent of **1**. In this next step, the zwitterion is proposed to break apart by undergoing cleavage of the carbon−oxygen bond to form the free tantalum oxo species, **5**, and a highly reactive vinylidene fragment which rapidly reacts with another equivalent of **1**. Upon extensive further rearrangement (as shown in Scheme 5) and loss of methane, the final products **19**, **20**, and **21** are formed.

Overall, formation of **19**, **20**, and **21** stoichiometrically requires a net loss of 1 equiv of $Cp_2Ta(═O)(CH_3)$ and CH_4 in each reaction. An alternative explanation for this could involve free H_2O reacting with **1**. However, our inability to trap or observe water leads us to believe that H_2O is not produced first and therefore cannot subsequently react with another equivalent of **1** to produce **5** and methane.

The mechanism proposed in Scheme 5 is further supported by low-temperature spectroscopic experiments that indicated the formation of unstable intermediates. This is also consistent with the ^{13}C and ^2H labeling reactions which were carried out, showing that the β-carbon and methyl carbon of the acetylide ligand arise from the tantalum center and not from a carbonyl ligand.

Mechanism of Formation of $Cp_2(CH_3)Ta(\mu\text{-}O)Ru_3(C_4H_4)(CO)_9$. The formation of complex **3** requires that a still different mechanism is operating in the reaction between **1** and $Ru_3(CO)_{12}$. However, we believe its initial steps are similar to the others reported here. As shown in Scheme 6, we suggest that the reaction is initiated by an overall cycloaddition between the Ta═CH_2 groups from two molecules of **1** and two CO ligands at separate Ru centers, probably through a zwitterionic species **26** that is similar to the one structurally characterized earlier in the reaction of $Cp_2(CH_3)Ta═CH_2$ with $C_3F_7Re(CO)_5$. Follow-

Scheme 7

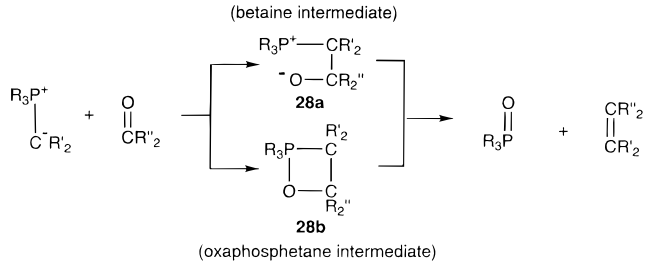

ing this step, two molecules of $Cp_2(CH_3)Ta{=}O$ are extruded to give the bis-vinylidene species **27**. Overall [2 + 2] cycloaddition of the Ru=C bonds then provides the carbon−carbon bond forming step necessary to reach a C_4H_4 fragment. We propose this complex then rapidly rearranges, as shown in Scheme 6, to give the final product **23**. During the reaction there must also be loss of CO and addition of one of the $Cp_2(CH_3)Ta(=O)$ fragments to the terminal Ru center, but it is unclear at which point in the overall transformation this occurs.

Mechanistic Summary

In spite of their overall diversity, the first and probably most important step involved in all the reactions observed here is the attack on a metal bound carbonyl by the methylidene species, **1**. Although this appears to be similar to a simple Wittig-type metathesis,[36] the mechanism is significantly different. The mechanism originally proposed for the Wittig reaction involves nucleophilic addition of a phosphorus ylide carbon to an organic carbonyl group to yield a dipolar (betaine) intermediate (intermediate **28a** in Scheme 7), followed by elimination of phosphine oxide. The elimination might be concerted, or it might take place via a four-membered oxaphosphetane intermediate (intermediate **28b** in Scheme 7).[37] Alternatively, this oxaphosphetane may be formed directly by a cycloaddition reaction of the ylide and the carbonyl compound, thus bypassing the betaine intermediate.[38,39] The formation of oxaphosphetanes at low temperature and their fragmentation on warming has been clearly demonstrated, while the evidence for authentic betaine intermediates has been questioned.[40] This betaine intermediate has recently come under renewed scrutiny, and current evidence does not favor this conventional pathway.[41,42] Although we propose a concerted first step to form an oxametallacyclobutane similar to the Wittig oxaphosphetane intermediate, to our knowledge a structure analogous to the zwitterionic species **16** has not been reported or proposed for the Wittig reaction. In addition, we have found no evidence to support ligand precoordination to the tantalum methylidene complex. Therefore, it is doubtful that attack by the methylidene carbon occurs after initial coordination of the carbonyl oxygen, as proposed in the insertion mechanisms of Stucky[43] and Grubbs,[3] who invoke precoordination of a carbonyl oxygen to electronically unsaturated early-metal centers.

Following the initial addition of the $Ta{=}CH_2$ to the CO ligand of the late-metal center and subsequent zwitterion formation, the reaction pathways apparently diverge depending on the metal center, the nuclearity of the cluster, and the ligand sphere of the metal. When the only ligands on the metal are CO's, the pathways seem to take one of two directions. Interestingly, there is a correlation between which pathway is taken and the distance between the two metal centers in the parent carbonyl complex. If the metal−metal bond length is relatively short in the ground state (such as $Fe_2(CO)_9$ (2.52 Å)[44] and $Co_2(CO)_8$ (2.52 Å)[45]) then the product obtained (e.g., **17** and **18**) contains two coupled carbonyls attached to the methylidene fragment. If the short bond length is retained in the critical intermediate, this may help the adjacent late-metal center to "swing" a second carbonyl oxygen into proximity for attack by the $OCCH_2$ group in **25** (Scheme 6).

The second observed pathway is seen when the metal−metal bond length is relatively long in the ground state (such as $Mn_2(CO)_{10}$ (2.9038(6) Å) or $Re_2(CO)_{10}$ (3.0413(11) Å))[46] or nonexistent (such as in the monomeric $Fe(CO)_5$ case). In these cases, the adjacent metal center (if there is one) apparently cannot bring a second carbonyl into the correct position to interact with the organic fragment. Instead, the $Cp_2Ta(=O)(CH_3)$ fragment in **22** (Scheme 5) breaks off upon cleavage of the remaining C−O bond of the zwitterionic fragment. This leaves a highly reactive vinylidene species bound to the late metal.

The coordination sphere is also important in determining the next step that the vinylidene takes and the ultimate structure of the organic fragment. If there is an alkyl or aryl group bound to the vinylidene late-metal center, solvent-induced migration of this group to the α-carbon of the vinylidene (e.g., **6a** → **8a** in Scheme 1) can occur. At this point the organic fragment is stabilized, but the late metal center still has a weakly coordinating solvent molecule bound to it. This solvent molecule can then be displaced by a better $2e^-$ donor such as the Ta=O species.

When there is no group other than a carbonyl ligand bound to the vinylidene late-metal fragment, then the system again can proceed in another direction. If there is only a mono- or dimeric metal fragment, the vinylidene rapidly reacts with a second equivalent of the methylidene ($Ta{=}CH_2$). The product of this reaction then undergoes extensive rearrangement and forms the bridging propynyl/carbonyl species with extrusion of methane (Scheme 5).

Finally, when the cluster is trimeric ($Ru_3(CO)_{12}$), the adjacent metal centers appear to be electron deficient enough to allow another carbonyl ligand to be attacked by a second equivalent of the tantalum methylidene. Upon extrusion of one more equivalent of "Ta=O", two vinylidene fragments couple with each other to form a C_4H_4 cumulene fragment. Loss of CO and coordination of "Ta=O" form the final cluster product (Scheme 6).

Conclusions

The rapid rate of these reactions appears to be a direct result of the interaction of two electronically different metal centers. Since all of these reported reactions occur in homogeneous solution, they have provided a unique opportunity to observe a number of organometallic intermediates which could possibly have analogs on heterogeneous surfaces during the Fischer−Tropsch process. It is unclear whether transformations exhibit-

(36) For a general review of the Wittig reaction, see: Maercker, A. *Org. React.* **1965**, *14*, 270.
(37) Trindle, C.; Hwang, J.-T.; Carey, F. A. *J. Org. Chem.* **1973**, *38*, 2664.
(38) For a theoretical study, see: Holler, R.; Lischkea, H. *J. Am. Chem. Soc.* **1980**, *100*, 4632.
(39) Vedejs, E.; Snoble, K. A. J. *J. Am. Chem. Soc.* **1973**, *95*, 5778.
(40) Vedejs, E.; Meier, G. P.; Snoble, K. A. J. *J. Am. Chem. Soc.* **1981**, *103*, 2823.
(41) Vedejs, E.; Marth, C. F. *J. Am. Chem. Soc.* **1990**, *112*, 3905.
(42) Maryanoff, B. E.; Reitz, A. B. *Chem. Rev.* **1989**, *89*, 863.
(43) Hamilton, D. M.; Willis, W. S.; Stucky, G. D. *J. Am. Chem. Soc.* **1981**, *103*, 4255.
(44) Cotton, F. A.; Troup, J. M. *J. Chem. Soc., Dalton Trans.* **1974**, 800.
(45) Sumner, G. G.; Klug, H. P.; Alexander, L. E. *Acta Crystallogr.* **1964**, *17*, 732.
(46) Churchill, M. R.; Amoh, K. N.; Wasserman, H. J. *Inorg. Chem.* **1981**, *20*, 1609.

ing related types of cleavage and rearrangement on surfaces proceed by mechanisms similar to those in the reactions described here, but the potential analogies are interesting.

Experimental Section

General. For a description of the instrumentation and general procedures used, please see an earlier paper from this laboratory.[47]

Unless otherwise specified, all reagents were purchased from commercial suppliers and used without further purification. Solid metal carbonyls were dried by stirring solutions of each over molecular sieves for several days and then subliming each twice. $Fe(CO)_5$ was distilled twice prior to use and stored at −30 °C in the absence of light. Pentane and hexanes (UV grade, alkene free) were distilled from sodium benzophenone ketyl/tetraglyme under nitrogen. Benzene, toluene, diethyl ether, and THF were distilled from sodium benzophenone ketyl under nitrogen. Deuterated solvents for use in NMR experiments were dried in the same way as their protiated analogs but were vacuum transferred from the drying agent. $Cp_2Ta(CH_2)(CH_3)$ (**1**),[10] $Cp_2Ta(C_2H_4)(CH_3)$,[10] $Ph_3P{=}{}^{13}CH_2$, $CH_3Re(CO)_5$ (**2a**),[48] $C_6H_5Re(CO)_5$ (**2b**),[48] and $C_3F_7Re(CO)_5$[49] were prepared by literature methods.

$Cp_2Ta(^{13}CH_2)(^{13}CH_3)$ (1-$^{13}C_2$). $Cp_2Ta(^{13}CH_2)(^{13}CH_3)$ was prepared in a fashion analogous to the literature method for **1**[10] except that $^{13}CH_3I$ was used in place of unlabeled CH_3I.

$Cp_2Ta(^{13}CH_2)(CH_3)$ (1-^{13}C). In the drybox, a solution of $Cp_2Ta(CH_3)(C_2H_4)$ (93.1 mg, 0.263 mmol) in THF (7 mL) was added to a quartz bomb (ca. 30 mL) equipped with a stirbar. A 5-mL THF solution of $Ph_3P{=}{}^{13}CH_2$ (72.6 mg, 0.262 mmol) was added dropwise to the bomb, and the solution was stirred magnetically for a few seconds. No color changes were observed. The bomb was then irradiated for 1 h at 0 °C with aliquots taken every 20 min to monitor the reaction (NMR). Upon complete conversion (> 95% by NMR) of the ethylene complex to the methylidene (**1**), the solution was concentrated to a brown gummy solid and redissolved in toluene (20 mL) and filtered through a 0.5-in. plug of silylated silica gel (Keiselgel 60). The filtrate was then layered with pentane (40 mL) and allowed to crystallize at −40 °C overnight. The tan crystals obtained were isolated and washed with 5 mL of cold pentane. The yield was 51.1 mg (56%). ^{1}H and ^{13}C NMR spectra showed >95% ^{13}C incorporation to the methylidene group and <5% incorporation of ^{13}C into the methyl group.[10]

$Re(CO)_5(CD_3)$ (2a-d_3). $Re(CO)_5(CD_3)$ was prepared in a fashion analogous to the literature method for **2a** except that CD_3I was used in place of the unlabeled CH_3I.

$Cp_2Ta(CH_3)(\mu$-O)Re(C(CH_3)=CH_2)(CO)$_4$ (3a). In a drybox, $Cp_2Ta(CH_2)(CH_3)$ (**1**) (155 mg, 0.456 mmol) dissolved in THF (5 mL) was added to a large vial equipped with a stirbar. Next, $CH_3Re(CO)_5$ dissolved in THF (5 mL) was added to the stirred solution of **1**, and the solution color immediately changed from brown to golden-brown. The solution continued to stir for 1 h and was concentrated *in vacuo*. The remaining residue was triturated with pentane (2 × 3 mL) and redissolved in benzene (12 mL). The C_6H_6 solution was then filtered through a 1-in. plug of silylated silica gel (Keiselgel 60), and the yellow filtrate was concentrated *in vacuo* to ca. 1 mL. The product was isolated by vapor diffusion of pentane into the remaining benzene solution which yielded 173 mg (61%) of golden platelike crystals of **3a**. NMR data for $Cp_2(CH_3)Ta(\mu$-O)Re(CCH_3=CH_2)(CO)$_4$ (**3a**): ^{1}H NMR (400 MHz, THF-d_8, 25 °C) δ 6.19 (s, 10H, C_5H_5), 5.99 (dq, 1H, $^2J_{HH}$ = 4.6 Hz, $^4J_{HH}$ = 1.0 Hz, CCH_2), 4.98 (dq, 1H, $^2J_{HH}$ = 4.6 Hz, $^4J_{HH}$ = 1.0 Hz, CCH_2), 2.29 (t, 3H, $^4J_{HH}$ = 1.0 Hz, CCH_3), 0.91 (s, 3H, TaCH_3); ^{13}C{^{1}H} NMR (101 MHz, THF-d_8, 25 °C) δ 195.4 (s, Re*C*O), 194.8 (s, Re*C*O), 193.9 (s, Re*C*O), 166.3 (s, Re*C*=CH_2), 122.2 (s, CCH_2), 111.7 (s, *C*$_5H_5$), 38.7 (s, C*C*H_3), 15.8 (s, Ta*C*H_3); MS (FAB) 682 (M^+), 654 (M^+ − CO), 626 (M^+ − 2CO). IR (KBr, cm^{-1}) 2918 (m), 2077 (m), 1965 (s), 1952 (s), 1896 (s), 1734 (m), 1570 (w), 1448 (w), 1435 (w), 1157 (w), 1024 (m), 897 (m), 835 (s), 615 (m), 594 (m). Anal. Calcd for $C_{18}H_{18}O_5TaRe$: C, 31.72; H, 2.66. Found: C, 31.99; H, 2.66.

$Cp_2Ta(CH_3)(\mu$-O)Re(C(CD_3)=CH_2)(CO)$_4$ (3a-d_3). In a drybox, $Cp_2Ta(CH_2)(CH_3)$ (**1**) (16.2 mg, 0.0476 mmol) dissolved in C_6D_6 (0.3 mL) was added to an NMR tube. Next, $CD_3Re(CO)_5$ dissolved in a minimum amount of C_6D_6 (ca. 0.4 mL) was added to the solution of **1**. The tube was capped and shaken, and a ^{1}H NMR spectrum was taken of the resulting golden solution after approximately 1 h of sitting at room temperature. The ^{1}H NMR showed a similar spectrum to that found for **3a** except that the resonance at δ 2.1 ppm was absent (<5% expected of the integration).

$Cp_2Ta(CH_3)(\mu$-O)Re(C(C_6H_5)=CH_2)(CO)$_4$ (3b). In a drybox, $Cp_2Ta(CH_2)(CH_3)$ (**1**) (200 mg, 0.590 mmol) dissolved in C_6H_6 (7 mL) was added to a large vial equipped with a stirbar. Next, $C_6H_5Re(CO)_5$ dissolved in C_6H_6 (5 mL) was added to the stirred solution of **1**, and the solution color immediately changed from brown to yellow. The solution was stirred for an additional 1 h and was then filtered through a 1.5-in. plug of silylated silica gel (Keiselgel 60); the yellow filtrate was concentrated *in vacuo* to ca. 1 mL. The product was isolated by vapor diffusion of pentane into the remaining benzene solution. After washing with pentane (2 × 3 mL) golden-yellow crystals of **3b** were obtained in a 260-mg yield (67%). NMR data for $Cp_2(CH_3)Ta(\mu$-O)-Re(CPh=CH_2)(CO)$_4$ (**3b**): ^{1}H NMR (400 MHz, C_6D_6, 25 °C) δ 7.46 (d, 2H, $^3J_{HH}$ = 7.0 Hz, *o*-C_6H_5), 7.30 (t, 1H, $^3J_{HH}$ = 7.8 Hz, *p*-C_6H_5), 7.06 (t, 2H, $^3J_{HH}$ = 7.3 Hz, *m*-C_6H_5), 6.53 (d, 1H, $^2J_{HH}$ = 4.6 Hz, CCH_2), 5.74 (d, 1H, $^2J_{HH}$ = 4.6 Hz, CCH_2), 5.28 (s, 10H, C_5H_5), 0.65 (s, 3H, TaCH_3); ^{13}C{^{1}H} NMR (101 MHz, THF-d_8, 25 °C) δ 194.0 (s, Re*C*O), 193.8 (s, Re*C*O), 193.1 (s, Re*C*O), 173.2 (s, Re*C*CH_2), 159.7 (s, CCH_2), 128.3 (s, *i*-C_6H_5), 126.5 (s, *o*-C_6H_5), 125.8 (s, *m*-C_6H_5), 124.2 (s, *p*-C_6H_5), 110.2 (s, *C*$_5H_5$), 15.9 (s, Ta*C*H_3); MS (FAB) 744 (M^+), 716 (M^+ − CO), 688 (M^+ − 2CO), 632 (M^+ − 4CO). Mp 96−99 °C. Anal. Calcd for $C_{23}H_{20}O_5TaRe$: C, 37.15; H, 2.71. Found: C, 37.23; H, 2.71.

Spectroscopic Observation of $Cp_2(CH_3)Ta(\mu$-O(CH_2)C=)Re-(CH_3)(CO)$_4$ (6a) and (H_2C=(CH_3)C)Re(CO)$_4$(THF-d_8) (8a). In the drybox, $CH_3Re(CO)_5$ (23.6 mg, 0.0691 mmol) and $Cp_2Ta(CH_2)(CH_3)$ (**1**) (23.1 mg, 0.0679 mmol) were weighed as crystalline solids into an NMR tube. The tube was attached to a cajon fitting and removed from the box. After being attached to a vacuum line, the tube was frozen in liquid N_2 and evacuated. Next, THF-d_8 (0.5 mL) was vacuum transferred in, and the tube was sealed. The tube was warmed to −78 °C at which point the crystals began dissolving. After dissolving as much as possible at this temperature, the tube was inserted into a precooled probe set at −50 °C; at this point ^{1}H NMR analysis showed little reaction. At −30 °C approximately 70% conversion to intermediate **6a** was observed. At 5 °C resonances for intermediate **8a**, $Cp_2Ta(CH_3)(=O)$ (**5**), and product **3a** were observed as the signal for intermediate **6a** began to decrease in intensity. Resonances for product **3a** continued to grow as resonances for **8a** and **5** decreased in intensity. Upon warming to room temperature, the only major resonances were attributable to the isolable product **3a** (>90%). ^{1}H NMR data for $Cp_2(CH_3)Ta(\mu$-O(CH_2)C=)Re(CH_3)(CO)$_4$ (**6a**) (400 MHz, THF-d_8, −20 °C): δ 6.52 (s, 10H, Cp), 4.32 (s, 1H, CH-*H*), 3.82 (s, 1H, CH-*H*), 1.16 (s, 3H, Ta-CH_3), −0.49 (s, 3H, Re-CH_3). ^{1}H NMR data for Re(C(CH_3)=CH_2)(CO)$_4$ (THF-d_8) (**8a**) (400 MHz, THF-d_8, 10 °C): δ 6.41 (dq, 1H, $^2J_{HH}$ = 4 Hz, $^4J_{HH}$ = 1 Hz, CH-*H*), 5.07 (dq, 1H, $^2J_{HH}$ = 4Hz, $^4J_{HH}$ = 1 Hz, CH-*H*), 2.33 (m, 3H, $^3J_{HH}$ = 1 Hz, C-CH_3).

Spectroscopic Observation of Re(C(CH_3)=CH_2)(PMe_3)(CO)$_4$ (10a). In the drybox, $Cp_2Ta(CH_2)(CH_3)$ (6.1 mg, 0.179 mmol) and $CH_3Re(CO)_5$ (6.8 mg, 0.020 mmol) were added as crystalline solids to an NMR tube. The tube was attached to a cajon fitting and removed from the box. After being attached to a vacuum line, the tube was frozen in liquid N_2 and evacuated. Next, THF-d_8 (0.6 mL) and PMe_3 (2.6 mg, 0.034 mmol) were vacuum transferred into the tube, and the tube was sealed. At this point the tube was treated similarly to the reaction described above to observe **6a** and **8a**. The same observations were made as above except that upon the final warming, the usual product **3a** was not observed, but the PMe_3 adduct **10a** was observed along with **5**. ^{1}H NMR of Re(PMe_3)(CO)$_4$(C(CH_3)=CH_2): ^{1}H NMR (400 MHz, THF-d_8, 25 °C) δ 6.40 (m, 1H, CCH_2), 5.04 (m, 1H, CCH_2), 2.34 (d, 3H, $^4J_{HH}$ = 1 Hz, CCH_3), 1.67 (d, 9H, $^2J_{PH}$ = 9.3 Hz, PCH_3); ^{31}P{^{1}H} NMR (THF-d_8, 25 °C) δ −37.5.

Re(C(CH_3)=CH_2)(CO)$_5$ (11a). (a) A NMR tube was charged with **3a** (9.4 mg, 0.014 mmol) and dry THF-d_8 (0.5 mL). The tube was

(47) Baranger, A. M.; Bergman, R. G. *J. Am. Chem. Soc.* **1994**, *116*, 3822.

(48) King, R. B. *Organometallic Syntheses*; Academic Press: New York, 1965; Vol. 1.

(49) McClellan, W. R. *J. Am. Chem. Soc.* **1961**, *83*, 1598.

attached to a vacuum line through a cajon fitting and frozen in liquid N_2. Next, the tube was pressurized with CO (2.4 atm), sealed, and allowed to warm to room temperature. After 24 h at ambient temperature a white flocculent solid characteristic of **5** had formed. The solid was centrifuged to the bottom of the tube and a ^{1}H NMR spectrum was taken showing the major product was **11a**. NMR of $Re(CO)_5(C(CH_3)=CH_2)$ (**11a**): ^{1}H NMR (400 MHz, THF-d_8, 25 °C) δ 5.76 (s(br), 1H, CH-*H*), 5.44 (s(br), 1H, CH-*H*), 1.65 (s(br), 1H, CC*H*$_3$).

(b) A procedure similar to that used in the formation of **10a** was used to form **11a** also except that CO (2.9 atm) was used in place of PMe_3 (91%). The ^{1}H NMR spectrum was identical to that given above.

(c) In a drybox, a THF (15 mL) solution of freshly prepared $NaRe(CO)_5$ (1.83 g, 5.24 mmol) in a large vial equipped with a stirbar was cooled to −40 °C. While stirring the solution rapidly, methacrolyl chloride (0.658 g, 6.30 mmol) was added dropwise. Upon warming, the solution color changed from red to yellow. After stirring for 1 h while warming to room temperature, the solution was concentrated *in vacuo* to a yellow solid. The product was then sublimed at 105 °C under vacuum onto a −78 °C cold finger to yield a mixture of $CH_2(CH_3)C(CO)Re(CO)_5$ and $CH_2(CH_3)CRe(CO)_5$ (**11a**) (1.266 g). The impure product was heated again in a sublimator under vacuum to 135 °C at which point there appeared to be gaseous evolution (CO) and pure product sublimation onto the cold finger. The pure product **11a** was then collected from the cold finger (0.957 g) in 48% overall yield. ^{1}H NMR of $CH_2(CH_3)C(CO)Re(CO)_5$ δ 6.12 (s(br), 1H, CH-*H*), 5.22 (s(br), 1H, CH-*H*), 2.36 (s(br), 3H, CC*H*$_3$). The ^{1}H NMR spectrum of $CH_2(CH_3)CRe(CO)_5$ was identical to that given above.

Generation of $Cp_2(CH_3)Ta(\mu\text{-}O)Re((C(CH_2))_2CH_3)(CO)_4$ (12a). In the drybox, $Cp_2Ta(CH_2)(CH_3)$ (**1**) (68.5 mg, 0.201 mmol) was dissolved in THF (15 mL) and cooled to −40 °C. A solution of $(CH_2)(CH_3)CRe(CO)_5$ (**11a**) (71.4 mg, 0.201 mmol) in THF (10 mL) was added dropwise to the stirred solution of **1**. The resulting yellow solution was allowed to warm to room temperature before the volatile materials were removed *in vacuo*, at which point the residue was redissolved in C_6H_6 (30 mL). This was then filtered through a 0.75-in. plug of silylated silica gel (Kieselgel 60). An aliquot of the filtrate was then used for a ^{1}H NMR. ^{1}H NMR of **12a** (400 MHz, C_6D_6) δ 6.47 (d, 1H, $^2J_{HH}$ = 4.0 Hz, ReCCH-*H*), 5.94 (d, 1H, $^2J_{HH}$ = 4.0 Hz, ReCCH-*H*), 6.26 (m, 1H, C(CH$_3$)CH*H*), 5.71 (m, 1H, C(CH$_3$)CH*H*), 5.43 (s, 10 H, C_5H_5), 2.12 (br, 3H, CC*H*$_3$), 0.60 (s, 3H, Ta-C*H*$_3$).

Generation of $Re((C(CH_2))_2CH_3)(CO)_5$ (13a). A procedure analogous to that used in the formation of **11a** (preparation (**a**)) was used to form **13a**. NMR of $Re((C(CH_2))_2CH_3)(CO)_5$ (**13a**): ^{1}H NMR (400 MHz, THF-d_8, 20 °C) δ 5.82 (s(br), 1H, CH-*H*), 5.57 (s(br), 1H, CH-*H*), 5.21 (s(br), 1H, CH-*H*), 5.05 (s(br), 1H, CH-*H*), 1.71 (s(br), 3H, CC*H*$_3$).

$Cp_2(CH_3)Ta(\mu\text{-}CH_2(O)C=)Re(C_3F_7)(CO)_4$ (16). In the drybox, a large vial (20 mL) equipped with a stirbar was charged with a solution of $C_3F_7Re(CO)_5$ (**15**) (54.5 mg, 0.110 mmol) dissolved in THF (5 mL) and cooled to −40 °C. Next, $Cp_2Ta(CH_2)(CH_3)$ (**1**) (40.1 mg, 0.118 mmol) was dissolved in THF (5 mL) and cooled to −40 °C. The solution of **1** was then added to the stirred solution of **15** and the resulting mixture was warmed slowly to 10 °C. At this point, the THF solution was concentrated *in vacuo* to ca. 3 mL and layered with 0.5 mL of cold THF and finally 3 mL of cold pentane. The vial was then allowed to stand at −40 °C in a pentane vapor diffusion recrystallization apparatus for 2 weeks during which time yellow crystals of product **16** formed (49 mg) in 53% yield. These crystals were suitable for a single-crystal X-ray diffraction analysis and were not allowed to warm to room temperature for more than 5 min (the thermal instability of this material also precluded elemental analysis). A second crop was obtained by layering further with 5 mL of cold pentane to yield another 18 mg (20%) of pure product (total yield: 67 mg, 73%). ^{1}H NMR (400 MHz, THF-d_8, 15 °C) δ 6.53 (s, 10H, C_5H_5), 4.46 (s(br), 1H, CH-*H*), 4.14 (s(br), 1H, CH-*H*), 1.28 (s, 3H, Ta-CH$_3$); ^{19}F{^{1}H} NMR (C_6D_6, 15 °C) δ −9.6 (q, 2F, Re-C*F*$_2$), −15.0 (t, 3F, CF$_2$C*F*$_3$), −51.8 (s, 2F, CF$_2$C*F*$_2$CF$_3$).

$Cp_2Ta(CH_3)(\mu\text{-}\eta^1\text{:}\eta^2\text{:}\eta^3\text{-}C_3H_2O_2)Co_2(CO)_6$ (17). In a drybox, $Co_2(CO)_8$ (36.0 mg, 0.0316 mmol) was slurried in THF (10 mL) in a round-bottom flask (50 mL) equipped with a stirbar. $Cp_2Ta(CH_2)(CH_3)$ (**1**) (35.2 mg, 0.103 mmol) was dissolved in THF (5 mL) and slowly added dropwise into the stirred slurry over a period of 5 min. The mixture remained brown in color during the 2 h of stirring at room temperature. The reaction mixture was then concentrated *in vacuo* and redissolved in C_6H_6 (15 mL). The solution was filtered through a 2-in. plug of silylated silica gel (Keiselgel 60) and the eluent was concentrated *in vacuo* to ca. 7 mL. Slow vapor diffusion of pentane into this benzene solution yielded 38 mg of dark brown crystals of **17** (55%) suitable for X-ray diffraction studies. ^{1}H NMR (400 MHz, C_6D_6, 25 °C) δ 5.23 (s, 5H, C_5H_5), 5.09 (s, 5H, C_5H_5), 3.12 (d, 1H, $^2J_{HH}$ = 2.5 Hz, CH-*H*), 2.49 (d, 1H, $^2J_{HH}$ = 2.6 Hz, CH-*H*), 0.65 (s, 3H, Ta-C*H*$_3$); ^{13}C{^{1}H} NMR (101 MHz, THF-d_8, 25 °C) δ 209.0 (s, *C*O), 207.8 (s(br), *C*O), 207.6 (s(br), *C*O), 204.2 (s(br), *C*O), 139.0 (s, C_2O_2), 129.0 (s, C_2O_2), 112.9 (s, C_5H_5), 112.8 (s, C_5H_5), 49.0 (s, *C*H$_2$), 36.8 (s, Ta-*C*H$_3$); FAB mass spec *m*/*z* = 626 [M − 2CO]$^+$, 570 [M − 4CO]$^+$, 542 [M − 5CO]$^+$, 514 [M − 6CO]$^+$, 499 [M − 6CO − CH$_3$]$^+$; IR (KBr, cm^{-1}) = 2057 (s), 2010 (s), 1992 (s), 1960 (s), 1946 (s), 1887 (m), 1734 (m). Anal. Calcd for $C_{22}H_{15}Co_2O_{10}Ta$: C, 35.22; H, 2.22. Found: C, 35.17; H, 2.13.

$Cp_2(CH_3)Ta(\mu\text{-}\eta^1\text{:}\eta^2\text{:}\eta^3\text{-}C_3H_2O_2)Fe_2(CO)_7$ (18). In a drybox, freshly sublimed $Fe_2(CO)_9$ (212. mg, 0.584 mmol) was slurried in THF (10 mL) and stirred rapidly, forming a faint orange slurry with solid $Fe_2(CO)_9$ floating in the mixture. $Cp_2Ta(CH_2)(CH_3)$ (**1**) (198 mg, 0.583 mmol) was dissolved in THF (7 mL) and slowly added dropwise into the stirred slurry over a period of 2 min. The mixture became homogeneous and turned a deep red color while it was stirred for 1 h. The volatile materials were removed *in vacuo* leaving a dark red residue which was washed with pentane (3 × 2 mL). The remaining residue was redissolved in C_6H_6 (15 mL) and the resulting red solution was filtered through a 0.5-in. plug of silylated silica gel (Keiselgel 60) and recrystallized from vapor diffusion of pentane into a saturated benzene solution of **18**. The crystals of **18** obtained were suitable for a single-crystal X-ray diffraction analysis and were obtained in 47% yield (197 mg). ^{1}H NMR (400 MHz, C_6D_6, 25 °C) δ 5.39 (s, 5H, C_5H_5), 5.16 (s, 5H, C_5H_5), 2.77 (d, 1H, $^2J_{HH}$ = 5.4 Hz, CH-*H*), 1.97 (d, 1H, $^2J_{HH}$ = 5.4 Hz, CH-*H*); ^{13}C{^{1}H} NMR (101 MHz, THF-d_8, 25 °C) δ 214.19 (s, *C*O), 198.40 (s, *C*O), 189.3 (s, *C*O), 144.4 (s, *C*O), 112.72 (s, C_5H_5), 112.61 (s, C_5H_5), 100.48 (s, C_2O_2), 89.20 (s, C_2O_2), 39.65 (s, *C*H$_2$), 36.38 (s, Ta-*C*H$_3$); MS (EI) *m*/*z* = 186 (FeCp$_2$)$^+$, 121 (FeCp)$^+$, (no Ta containing fragments were found); MS (FAB) *m*/*z* = 704 [M]$^+$, 676 [M − CO]$^+$, 648 [M − 2CO]$^+$, 620 [M − 3CO]$^+$, 592 [M − 4CO]$^+$, 577 [M − 4CO − CH$_3$]$^+$, 564 [M − 5CO]$^+$, 536 [M − 6CO]$^+$, 508 [M − 7CO]$^+$, 493 [M − 7CO − CH$_3$]$^+$; IR (KBr, cm^{-1}) 2075 (s), 1998 (s), 1968 (s), 1949 (s), 1730 (m). Anal. Calcd for $C_{21}H_{15}Fe_2O_9Ta$: C, 35.83; H, 2.15. Found: C, 35.76; H, 2.30.

$Cp_2Ta(\mu\text{-}CO)(\mu\text{-}\eta^1\text{:}\eta^2\text{-}C_3H_3)Re(CO)_3Re(CO)_5$ (19). In a drybox, $Cp_2Ta(CH_2)(CH_3)$ (**1**) (212 mg, 0.624 mmol) was dissolved in THF (4 mL) and added to a large vial (20 mL) equipped with a stirbar. Then, $Re_2(CO)_{10}$ (396 mg, 0.606 mmol) was dissolved in THF (8 mL) and slowly added dropwise to the stirred solution of $Cp_2Ta(CH_2)(CH_3)$. The resulting solution turned red after a few seconds and after 5 min the solution was reddish-brown. The solution was stirred for a total of 35 min and was concentrated *in vacuo* to an orange solid. This solid was washed with pentane (2 × 10 mL) leaving a light orange powder. Dark orange crystals were isolated by THF/pentane layering and slow cooling to −40 °C to yield 366 mg of crystalline solid (62%) suitable for X-ray diffraction studies. ^{1}H NMR (400 MHz, THF-d_8, 25 °C) δ 5.27 (s, 10H, C_5H_5), 3.01 (s, 3H, C*H*$_3$); ^{13}C{^{1}H} NMR (101 MHz, THF-d_8, 25 °C) δ 266.53 (s, μ-*C*O), 200.57 (s, *C*O), 197.65 (s, *C*O), 197.40 (s, *C*O), 139.69 (s, $^1J_{CC}$ = 101.4 Hz, $^2J_{CC}$ = 5.0 Hz, $^3J_{CH}$ = 6.0 Hz, Ta-*C*-Re), 127.74 (s, $^1J_{CC}$ = 101.4 Hz, $^2J_{CH}$ = 8.0 Hz, *C*-CH$_3$), 102.35 (s, C_5H_5), 18.71 (s, $^1J_{CH}$ = 128.8, $^2J_{CC}$ = 5.0 Hz, C≡C-*C*H$_3$); MS (FAB) *m*/*z* = 974 [M]$^+$, 918 [M − 2CO]$^+$, 890 [M − 3CO]$^+$, 862 [M − 4CO]$^+$, 834 [M − 5CO]$^+$, 807 [M − 5CO − CCH$_3$]$^+$, 778 [M − 7CO]$^+$, 750 [M − 8CO]$^+$; IR (KBr, cm^{-1}) 2097 (s), 2070 (s), 2030 (s), 2007 (s), 1994 (s), 1980 (s), 1921 (s), 1847 (m), 1713 (s). Anal. Calcd for $C_{22}H_{13}Re_2O_9Ta$: C, 27.11; H, 1.34. Found: C, 27.06; H, 1.38.

$Cp_2Ta(\mu\text{-}CO)(\mu\text{-}\eta^1\text{:}\eta^2\text{-}C_3H_3)Mn(CO)_3Mn(CO)_5$ (20). A procedure similar to the one used to prepare **19** was used to prepare **20** except $Cp_2Ta(CH_2)(CH_3)$ (**1**) (76.1 mg, 0.223 mmol) and $Mn_2(CO)_{10}$ (43.3 mg, 0.111 mmol) were used. Yield 46 mg (58%). ^{1}H NMR (400 MHz, C_6D_6, 25 °C) δ 4.52 (s, 10H, C_5H_5), 2.47 (s, 3H, C*H*$_3$); ^{13}C{^{1}H} NMR

(101 MHz, THF-d_8, 20 °C) δ 268.1 (s, μ-*C*O), 201.9 (s, *C*O), 199.4 (s, *C*O), 195.3 (s, *C*O), 148.1 (s, Ta-*C*-Mn), 123.5 (s, *C*-CH_3), 108.5 (s, C_5H_5), 20.8 (s, C≡C-*C*H_3); MS (FAB) *m*/*z* = 712 $[M]^+$, 628 $[M - 3CO]^+$, 600 $[M - 4CO]^+$, 517 $[M - Mn(CO)_5]^+$, 461 $[M - Mn - 7CO]^+$, 405 $[M - Mn - 9CO]^+$, 350 $[M - Mn_2(CO)_9]^+$; IR (KBr, cm^{-1}) 2075 (s), 2015 (s), 1986 (s), 1957 (s), 1916 (s), 1722 (s). Anal. Calcd for $C_{22}H_{13}Mn_2O_9Ta$: C, 37.10; H, 1.84. Found: C, 36.76; H, 2.02.

$Cp_2Ta(\mu\text{-}CO)(\mu\text{-}\eta^1\text{:}\eta^2\text{-}C_3H_3)Fe(CO)_3$ (21). In a drybox, $Cp_2Ta(CH_2)(CH_3)$ (**1**) (529 mg, 1.55 mmol) was dissolved in THF (13 mL) and transferred to a glass bomb equipped with a stirbar. The bomb was removed from the box, attached to a vacuum line, and degassed by 3 freeze−pump−thaw cycles. Next, $Fe(CO)_5$ (152 mg, 0.777 mmol) was vacuum transferred into the bomb which was frozen in liquid N_2. The bomb was allowed to warm slowly to room temperature with constant stirring, and it was then stirred for another 10 min. The red-brown solution was concentrated *in vacuo* and the residue was extracted with benzene (21 mL). The resulting solution was filtered through a 1-in. plug of silylated silica gel (Keiselgel 60) affording a reddish-orange filtrate which was concentrated to ca. 10 mL. The product **21** was recrystallized using a benzene/pentane vapor diffusion apparatus and was isolated in 47% yield (189 mg). ^{1}H NMR (400 MHz, C_6D_6, 25 °C) δ 4.45 (s, 10H, C_5H_5), 2.413.01 (s, 3H, CH_3); $^{13}C\{^1H\}$ NMR (101 MHz, THF-d_8, 25 °C) δ 288.99 (s, μ-*C*O), 218.20 (s(br), *C*O), 153.85 (s, Ta-*C*-Fe), 123.11(s, *C*-CH_3), 101.89 (s, C_5H_5), 18.34 (s, C≡C-*C*H_3); MS (FAB) *m*/*z* = 518 $[M - CO]^+$, 490 $[M - 2CO]^+$, 462 $[M - 3CO]^+$; IR (KBr, cm^{-1}) 2000 (s), 1938 (s), 1915 (s), 1886 (sh), 1732 (s), 1714 (s). Anal. Calcd for $C_{17}H_{13}FeO_4Ta(0.5\ C_6H_6)$: C, 43.11; H, 2.87. Found: C, 42.89; H, 2.48.

Generation of $Cp_2(CH_3)Ta(\mu\text{-}O(CH_2)C)Re_2(CO)_9$ (22). In a drybox, $Cp_2Ta(CH_2)(CH_3)$ (22.3 mg, 65.5 μmol) and $Re_2(CO)_{10}$ (23.5 mg, 36.1 μmol) were added to a NMR tube as crystalline solids. The tube was attached to a cajon fitting and after being removed from the box, it was degassed on a vacuum line. While the tube was frozen in liquid N_2, THF-d_8 (0.5 mL) was vacuum transferred into the tube, and the tube was sealed. The tube was thawed and warmed to −78 °C at which point it was shaken vigorously. Compound **1** dissolved completely, but the $Re_2(CO)_{10}$ only dissolved partially. At this point the tube was treated similarly to the reaction described above to observe **6a** and **8a**. Resonances for the intermediate **22** were observed initially at −35 °C and did not begin to disappear until ca. 0 °C. ^{1}H NMR for $Cp_2(CH_3)Ta(\mu\text{-}O(CH_2)C)Re_2(CO)_9$ (**22**) (400 MHz, THF-d_8, −5 °C) δ 6.52 (s, 10H, C_5H_5), 4.27 (s(br), 1H, CH-*H*), 4.12 (s(br), 1H, CH-*H*), 1.26 (s, 3H, CH_3).

Scrambling Experiment with 1-^{13}C and $Re_2(CO)_{10}$. An experiment identical to that used to generate **22** was performed except that **1-^{13}C** was used in place of **1**. Upon the initial signs of reaction, the starting material began to show resonances for both $Cp_2Ta(^{13}CH_2)(CH_3)$ and $Cp_2Ta(CH_2)(^{13}CH_3)$ in approximately equal amounts. The product obtained (**19**) had enriched ^{13}C-resonances in the β- and γ- positions of the methyl acetylide ligand.

$Cp_2(CH_3)Ta(\mu\text{-}O)Ru_3(\mu\text{-}\eta^1\text{:}\eta^1\text{:}\eta^3\text{-}C_4H_4)(CO)_9$ (23). A THF (5 mL) solution of $Cp_2Ta(CH_2)(CH_3)$ (76.2 mg, 0.224 mmol) at 0 °C was added dropwise to a rapidly stirred slurry of $Ru_3(CO)_{12}$ (138 mg, 0.217 mmol) in THF (12 mL) in a large vial at 0 °C. The slurry turned deep red/brown and was stirred for a period of 25 min with slow warming to room temperature. The slurry was then filtered to remove excess starting $Ru_3(CO)_{12}$. The filtrate was concentrated *in vacuo* leaving a brown residue. This residue was extracted with C_6H_6 (ca. 20 mL) and filtered through a 1-in. silylated silica gel plug (Kieselgel 60). The yellow filtrate was then concentrated *in vacuo* to ca. 5 mL, and the product was recrystallized from vapor diffusion of pentane into a saturated benzene solution of **23**. The yellow crystals of **23** which formed were isolated (34.1 mg) in 32% yield. NMR data for $Cp_2(CH_2)Ta(\mu\text{-}O)Ru_3(C_4H_4)(CO)_9$ (**23**): ^{1}H NMR (400 MHz, C_6D_6, 25 °C) δ 5.17 (s, 5H, C_5H_5), 5.10 (s, 5H, C_5H_5), 4.39 (d, 1H, $^2J_{HH}$ = 2.6 Hz, CH_2), 4.26 (d, 1H, $^2J_{HH}$ = 2.5 Hz, CH_2), 2.00 (d, 1H, $^2J_{HH}$ = 1.3 Hz, CH_2), 1.51 (d, 1H, $^2J_{HH}$ = 1.3 Hz, CH_2), 0.35 (s, 3H, Ta-CH_3); $^{13}C\{^1H\}$ NMR (101 MHz, THF-d_8, 25 °C) δ 208.6 (s, Ru-*C*O), 201.9 (s, Ru-*C*O), 200.3 (s, Ru-*C*O), 199.8 (s, Ru-*C*O), 199.1 (s, Ru-*C*O), 195.3 (s, Ru-*C*O), 190.2 (s, Ru-*C*O), 143.4 (s, H_2CCCCH_2), 112.0 (s, C_5H_5), 111.9 (s, C_5H_5), 85.1 (s, H_2CCCCH_2), 66.7 (s, CH_2), 18.6 (s, CH_2), 15.7 (s, CH_3); MS (FAB) *m*/*z* 950.8 $[M^+]$, 922.8 $[M^+ - CO]$, 894.7 $[M^+ - 2CO]$, 866.7 $[M^+ - 3CO]$, 838.7 $[M^+ - 4CO]$, 782.7 $[M^+ - 6CO]$, 500.0 $[M^+ - Ru_2(CO)_7(C_4H_4)]$, 472.0 $[M^+ - Ru_2(CO)_8(C_4H_4)]$, 444.0 $[M^+ - Ru_2(CO)_9(C_4H_4)]$. Anal. Calcd for $C_{24}H_{17}O_{10}TaRu_3(0.5\ C_6H_6)$: C, 32.80; H, 2.04. Found: C, 32.75; H, 2.42.

X-ray Crystal Structure Determinations. A detailed description of the crystallographic analysis of **23** is given below. However, the structures of compounds **3b**, **16**, **17**, **18**, **19**, **20**, and **21** were solved similarly, and for brevity only a short description of the experimental details of the analyses of these compounds is presented.

X-ray Crystallographic Analysis of $Cp_2(CH_3)Ta(\mu\text{-}O)Ru_3(\mu\text{-}\eta^1\text{:}\eta^1\text{:}\eta^3\text{-}C_4H_4)(CO)_9$ (23). Yellow crystals, shaped as blocks and points, were obtained by slow crystallization from benzene/pentane vapor diffusion as described above. A fragment cut from one of these crystals was mounted on a glass fiber using Paratone N hydrocarbon oil. The crystal was then transferred to an Enraf-Nonius CAD-4 diffractometer and centered in the beam. It was cooled to −83 °C by a nitrogen-flow low-temperature apparatus which had been previously calibrated by a thermocouple placed at the sample position. Automatic peak search and indexing procedures yielded a triclinic reduced primitive cell. Inspection of the Niggli values revealed no conventional cell of higher symmetry.

The 5126 unique raw intensity data were converted to structure factor amplitudes and their esd's by correction for scan speed, background, and Lorentz and polarization effects. No correction for crystal decomposition was necessary. Inspection of the azimuthal scan data showed a variation I_{min}/I_{max} = 0.63 for the average curve. However, examination of several of the azimuthal scans showed a pattern of misorientation which was not accounted for in the accepted scans. The structure was solved initially with data corrected by the azimuthal scan data, but the final absorption correction was an empirical correction based on the combined differences of F_{obs} and F_{clc} following refinement of all atoms with isotropic thermal parameters (Corr(max) = 1.16, Corr(min) = 0.87).[50] The choice of the centric group P was confirmed by the successful solution and refinement of the structure. Removal of 77 data affected by misorientation just prior to a recalculation of the orientation matrix during data collection left 4980 unique data in the final data set.

The structure was solved by Patterson methods and refined via standard least-squares and Fourier techniques. In a difference Fourier map calculated following the refinement of all non-hydrogen atoms with anisotropic thermal parameters, peaks were found corresponding to the positions of most of the hydrogen atoms. Hydrogen atoms were assigned idealized locations and values of B_{iso} approximately 1.3 times the B_{eqv} of the atoms to which they were attached. They were then allowed to refine with isotropic thermal parameters. The methylene hydrogens on the ligand were located on a subsequent difference Fourier map and also allowed to refine. In the final cycles of least squares, 24 data with abnormally large weighted difference values (possibly caused by multiple diffraction effects) were given zero weight.

The final residuals for 451 variables refined against the 4112 accepted data for which $F^2 > 3\sigma(F^2)$ were R = 2.24%, wR = 2.27%, and GOF = 1/245. The R value for all 4956 accepted data was 3.35%. In the final cycles of refinement a secondary extinction parameter[51] was included (maximum correction: 15% on F).

The *p*-factor, used to reduce the weight of intense reflections, was set to 0.02 in the last cycles of refinement. The analytical forms of the scattering factor tables for the neutral atoms were used[52] and all scattering factors were corrected for both the real and imaginary components of anomalous dispersion.

The largest peak in the final difference Fourier map had an electron density of 0.75 $e^-/Å^3$, and the lowest excursion −0.22 $e^-/Å^3$. All large peaks were located near the metal atoms.

X-ray Crystallographic Analyses of 3b, 16, 17, 18, 19, 20, and 21. Crystals of compounds **3b**, **16**, **17**, **18**, **19**, **20,** and **21** were grown as described in the respective syntheses of each compound. The crystal mounting procedures and diffractometer were similar to that described

(50) Walker, N.; Stuart, D. *Acta Crystallogr.* **1983**, *A39*, 159.
(51) Zachariesen, W. H. *Acta Crystallogr.* **1963**, *16*, 1139.
(52) Cromer, D. T.; Waber, J. T. *International Tables for X-Ray Crystallography*; The Kynoch Press: Birmingham, England, 1974; Vol. IV.

for **23**, and the specific data collection parameters for these data sets are given in the tables referred to in the Results section. Automatic peak search and indexing procedures yielded the primitive cells.

The raw intensity data were converted to structure factor amplitudes and their esd's by correction for scan speed, background, and Lorentz and polarization effects. No corrections for crystal decomposition were necessary. An empirical correction based on the observed variation in the azimuthal scan data was applied. Removal of systematically absent data left the unique data in the final data set. The structures were solved by Patterson methods and refined via standard least-squares and Fourier techniques. The analytical forms of the scattering factor tables for the neutral atoms were used and all scattering factors were corrected for both the real and imaginary components of anomalous dispersion.

Acknowledgment. We acknowledge the National Science Foundation (Grant No. CHE-9113261) for generous financial support of this work and Dr. F. J. Hollander, director of the University of California Berkeley X-ray diffraction facility (CHEXRAY), for the determination of the X-ray structures. G.P. acknowledges the Department of Education for a predoctoral fellowship. We are also grateful to Dr. M. J. Hostetler for carrying out some initial reactions in this work. Finally, we appreciate an unusually detailed reading and annotation of the paper, as well as a persuasive suggestion for the mechanism of formation of **21**, by a referee.

Supporting Information Available: Tables containing crystal and data collection parameters, positional parameters, and anisotropic temperature factors for **3b**, **16**, **17**, **18**, **19**, **20**, **21** and **23** (14 pages). This material is contained in many libraries on microfiche, immediately follows this article in the microfilm version of the journal, can be ordered from the ACS, and can be downloaded from the Internet; see any current masthead page for ordering information and Internet access instructions.

JA951685J